A Tensor Artificial Viscosity using a Mimetic Finite Difference Algorithm

J. Campbell and M. Shashkov
Los Alamos National Laboratory
T-7, MS-B284
Los Alamos NM 87545

April 2000

LA-UR-00-2290

Abstract

We have developed a multi-dimensional tensor artificial viscosity for finite difference shock wave computations on a logically rectangular grid. The discrete viscosity tensor is formed by multiplying the gradient of velocity tensor by a scalar term. The scalar term is based on the form of viscosity first presented by Kurapatanko, and also contains an advection limiter term. Mimetic discretizations are used to derive forms of the momentum and energy equations for a nonorthogonal grid with the viscosity tensor evaluated at the zone edges or median mesh edges. Calculating the artificial viscosity tensor at these locations allows advection limiters to be easily incorporated, these switch off the viscosity for self-similar motion. Results are presented for several test problems.

1 Introduction

The governing equations in a hydrodynamics code are the conservation equations. For a Lagrangian code the equations of conservation of mass (1.1), momentum (1.2) and energy (1.3) are written

$$\frac{1}{\rho}\frac{d\rho}{dt} = -\nabla \cdot \mathbf{v} \ , \tag{1.1}$$

$$\rho\frac{d\mathbf{v}}{dt} = -\nabla P \ , \tag{1.2}$$

$$\rho\frac{de}{dt} = -P \ \nabla \cdot \mathbf{v} \ , \tag{1.3}$$

where ρ is density, P is pressure, e is specific internal energy and $\mathbf{v}$ in the velocity vector.

If the hydrodynamics code is intended to solve problems involving shock waves then special methods are required to model the shock wave as, without these, post-shock oscillation will destroy the solution. A standard method is the introduction of an artificial viscosity term.

The pioneering artificial viscosity was developed by von Neumann and Richtmyer [1] for one dimensional shock wave calculations. Their approach was to modify the momentum and energy equations by adding a dissipative, viscosity like, term to the pressure that would produce a shock wave thickness on the order of to the spacing of the computational mesh. This term could be any function that satisfied the following constraints: the modified conservation equations must possess solutions without discontinuities, the Hugoniot equations must hold when all other dimensions are large compared to the shock thickness, and the dissipative term must be negligible outside of the shock wave. Their viscosity had the form

$$q = -\rho\Delta\mathbf{v}|\Delta\mathbf{v}| \ . \tag{1.4}$$

This term is quadratic in $\Delta\mathbf{v}$, is positive in compression and negative in expansion. As expansion does not require the viscosity term to give a stable solution, it is common to set $q = 0$ when $\Delta\mathbf{v} > 0$.

When using (1.4) nonphysical oscillations were still seen behind the shock wave. To remove these oscillations Landshoff [2] added a second term to q that was linear in $\Delta\mathbf{v}$ and so vanished less rapidly behind a shock wave

$$q = c_L\rho c_s|\Delta\mathbf{v}| + c_Q\rho(\Delta\mathbf{v})^2 \tag{1.5}$$

here c_s is the local sound speed and c_L and c_Q are non-dimensional constants, c_L multiplying the linear term and c_Q the quadratic. This basic form of viscosity has become widely used.

Another form of the viscosity term was described by Wilkins [3] who attributed it to Kurapatenko [4].

$$q_{Kur} = \rho \left\{ c_2 \frac{(\gamma - 1)}{4} |\Delta \mathbf{v}| + \sqrt{c_2^2 \left(\frac{\gamma - 1}{4} \right)^2 (\Delta \mathbf{v})^2 + c_1^2 c_s^2} \right\} |\Delta \mathbf{v}| \tag{1.6}$$

where c_1 and c_2 are non-dimensional constants, and γ is the ratio of specific heats. This expression will be referred to as the Kurapatenko form of viscosity. The expression was derived from the pressure jump across a shock in an ideal gas. With $c_1 = c_2 = 1$, ρ and c_s the density and sound speed ahead of the shock and $\Delta \mathbf{v}$ the velocity jump across the shock, the equation gives the pressure jump across it. Equation (1.6) reduces to the linear term of the basic shock viscosity as $\Delta \mathbf{v} \to 0$ and the quadratic term as $c_s \to 0$ or when $\Delta \mathbf{v}$ becomes large.

In a one dimensional calculation $\Delta \mathbf{v}$ is clearly defined. The simplest extension to n dimensions is to treat the viscosity as a pressure term and set $\Delta \mathbf{v} \approx \sqrt[n]{V}(\nabla \cdot \mathbf{v})$, where V is the zone volume. A more accurate extension is to take the velocity jump across the zone in the direction of the shock, but reliably calculating the shock direction is difficult and can introduce problems of its own. For a review of viscosity formulations see Benson [5].

Recently Caramana et al. [6] specified five properties that an artificial viscosity should possess, these are

1. Dissipativity: The artificial viscosity must only act to decrease kinetic energy.
2. Galilean invariance: The viscosity should vanish smoothly as the velocity field becomes constant.
3. Self-similar motion invariance: The viscosity should vanish for uniform contraction and rigid rotation.
4. Wave-front invariance: The viscosity should have no effect along a wave front of constant phase, on a grid aligned with the shock wave.
5. Viscous force continuity: The viscous force should go to zero continuously as compression vanishes and remain zero for expansion.

In the same paper they present an edge viscosity for Lagrangian codes which satisfies these conditions. A common test problem for shock wave codes is the Noh problem [7], where a volume of gas is given an initial inward radial velocity and a strong shock wave is generated at the point of convergence. Results presented for this problem in [6] deal with Lagrangian grids aligned with the flow. However with an initially square grid, jets are formed along the axes which results in a highly deformed mesh. Our opinion is that the reason for this is that the edge viscosity [6] does not model physical viscosity, and therefore does not have a well defined continuum limit. As a consequence it has a very random dependence on the grid.

The aim of the work described here was to develop a viscosity which retains the useful features of the edge viscosity, but is based on an approximation to physical viscosity which has the form

$$\mathbf{Q} = \mu \mathbf{D} \tag{1.7}$$

where $\mathbf{Q}$ is the viscous stress tensor, μ is the viscosity coefficient and $\mathbf{D}$ is the symmetric strain rate tensor

$$\mathbf{D} = \frac{1}{2}(\nabla \mathbf{v} + \nabla \mathbf{v}^{\mathrm{T}}) \ . \tag{1.8}$$

As an artificial viscosity stress tensor does not have to be symmetric, it is also possible to consider a viscosity of the form

$$\mathbf{Q} = \mu \mathbf{G}^{\mathrm{T}} \tag{1.9}$$

where $\mathbf{G} = \nabla \mathbf{v}$. For these two form of artificial viscosity the momentum equation, (1.2), becomes

$$\rho \frac{d\mathbf{v}}{dt} = -\nabla P + \nabla \cdot \mu \mathbf{D} \quad , \quad \rho \frac{d\mathbf{v}}{dt} = -\nabla P + \nabla \cdot \mu \mathbf{G} \tag{1.10}$$

for the symmetric and nonsymmetric viscosities respectively.

As we show by numerical experiment, using a tensor viscosity with these basic forms reduces dependence of the numerical solution on the grid.

The next section gives a brief description of the Caramana edge viscosity, and shows results from the Noh problem an initial square grid. Section 3 discusses the general form of the viscosity, and what constraints must be placed on the form of the viscosity coefficient in order to satisfy the five properties. In section 4 expressions for the divergence of a tensor and gradient of a vector in a general curvilinear coordinate system are derived. These expressions are then used in section 5 to develop the discrete operators required to implement the tensor viscosity. Then section 6 describes the actual form of viscosity coefficient used, and the implementation of the viscosity in the test code. In section 7 each of the test problems is described, and the results presented. Finally mesh and contour plots for each test problem are shown in the appendix.

2 Edge Viscosity

In this section we briefly describe the edge viscosity developed by Caramana et al. [6], and introduce some notations which we will use later.

We assume a logically rectangular mesh, so every zone is a quadrilateral and each internal node has four neighbor zones. A typical zone is shown in Fig. 1a. Each zone is subdivided by the median mesh which connects the center of the zone to the middle of each edge. The median mesh defines the control volume used to calculate the nodal forces through the momentum equation, Fig. 1b.

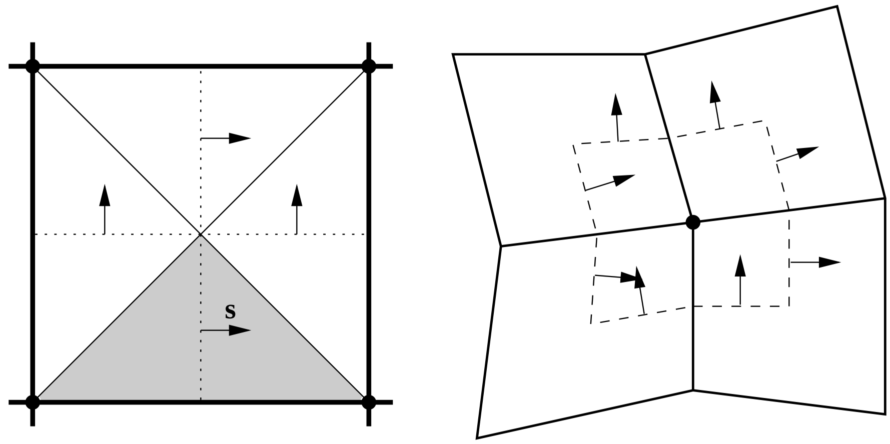

Fig. 1: (a): A quadrilateral zone. The solid lines show the boundaries of the triangular subzones, one subzone is shaded. The dotted lines show the median mesh. The vectors normal to the median mesh, $\mathbf{s}$, are defined as positive in the direction shown. (b): Integration path around median mesh for central node.

The vector $\mathbf{s}$ is the normal to the median mesh, the magnitude of the vector is equal to the length of the associated section of the median mesh.

For the edge viscosity each zone is split into four triangular subzones, each defined by then two nodes on an edge and the zone center Fig. 1a. The viscosity "tensor" is taken to be constant inside each of these subzones. The nodal acceleration can then be calculated using the conventional finite difference method of integrating around the median mesh surrounding each node. The median mesh is an eight-sided figure and the viscosity "tensor" is constant along each side.

For the subzone in zone z associated with edge k the viscosity "tensor" has the form

$$\mathbf{Q}_{z,k} = \begin{cases} (1-\psi_k) q_{kur,k} \widehat{\Delta\mathbf{v}_k} \widehat{\Delta\mathbf{v}_k} & \text{if} \quad \Delta\mathbf{v}_k \cdot \mathbf{s}_{z,k} \leq 0 \\ \\ 0 & \text{if} \quad \Delta\mathbf{v}_k \cdot \mathbf{s}_{z,k} > 0 \ . \end{cases} \tag{2.1}$$

In this equation $\Delta\mathbf{v}_k$ is the velocity difference between the two nodes at either end of edge k, $\widehat{\Delta\mathbf{v}_k}$ is the unit vector in the direction of this velocity difference. The two nodes at either end of edge k are b and c, Fig. 2. For the edge the density and sound speed are

$$\rho_k = \frac{2\rho_b\rho_c}{\rho_b + \rho_c} \ , \tag{2.2}$$

$$c_{s,k} = \min(c_{s,b}, c_{s,c}) \ . \tag{2.3}$$

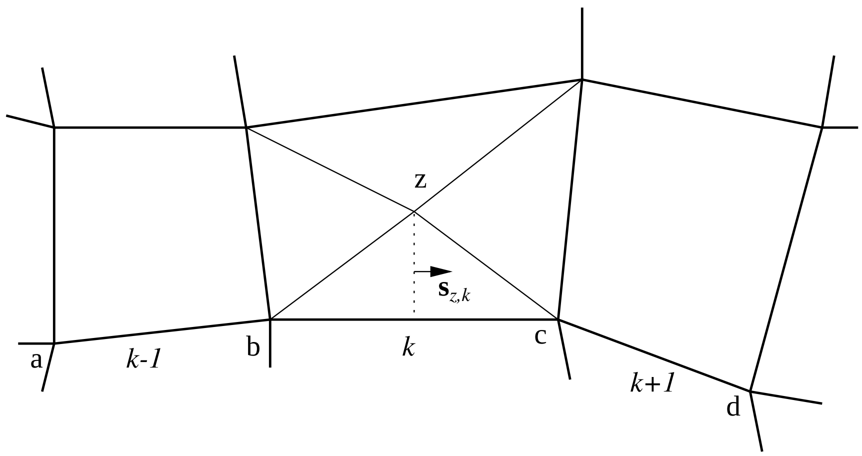

Fig. 2: A section of a logical mesh showing edge k and its neighbor edges.

The density and sound speed at a node is the volume weighted average of the surrounding zones. The final term to define is ψ_k which is a limiter function that acts to switch off the viscosity for self-similar motion and along wave fronts of constant phase. The function is defined as

$$\psi_k = \max[0, \min(0.5(r_{l,k} + r_{r,k})\ ,\ 2r_{l,k}\ ,\ 2r_{r,k}\ ,\ 1)]\ , \tag{2.4}$$

$$r_{r,k} = \frac{\Delta\mathbf{v}_{k+1}\cdot\widehat{\Delta\mathbf{v}_k}}{\Delta\mathbf{x}_{k+1}\cdot\widehat{\Delta\mathbf{x}_k}}\Bigg/\frac{|\Delta\mathbf{v}_k|}{|\Delta\mathbf{x}_k|}\quad ,\quad r_{l,k} = \frac{\Delta\mathbf{v}_{k-1}\cdot\widehat{\Delta\mathbf{v}_k}}{\Delta\mathbf{x}_{k-1}\cdot\widehat{\Delta\mathbf{x}_k}}\Bigg/\frac{|\Delta\mathbf{v}_k|}{|\Delta\mathbf{x}_k|}\quad . \tag{2.5}$$

Fig. 2 shows how the left and right edges are defined on a logical grid.

The term ψ is a multi-dimensional form of a one dimensional TVD advection limiter. The limiter is used to switch off the viscosity when the second derivative of the velocity field is zero and had the advantage that the second derivative does not have to be actually calculated. The limiter term ensures that the viscosity satisfies the conditions of self-similar motion invariance and wave front invariance.

The force due to the viscosity in the subzone z, k is

$$\mathbf{f}_{z,k} = \begin{cases} (1-\psi_k)q_{kur,k}(\widehat{\Delta\mathbf{v}_k}\cdot\mathbf{s}_{z,k})\widehat{\Delta\mathbf{v}_k} & \text{if} \quad (\Delta\mathbf{v}_k\cdot\mathbf{s}_{z,k}) \le 0 \\ 0 & \text{if} \quad (\Delta\mathbf{v}_k\cdot\mathbf{s}_{z,k}) > 0\ . \end{cases} \tag{2.6}$$

The edge viscosity satisfies the condition of Galilean invariance as the force is an explicit function of $\Delta\mathbf{v}_k$. Viscous force continuity is satisfied because the on/off switch $(\Delta\mathbf{v}_k\cdot\mathbf{s}_{z,k})$ also appears in the force expression.

The contribution from the viscous force in a subzone to the zone internal energy is $-\mathbf{f}_{z,k}\cdot\Delta\mathbf{v}_k$, $\mathbf{f}_{z,k}$ is proportional to $|\Delta\mathbf{v}_k|$, and is only non-zero if $\Delta\mathbf{v}_k$

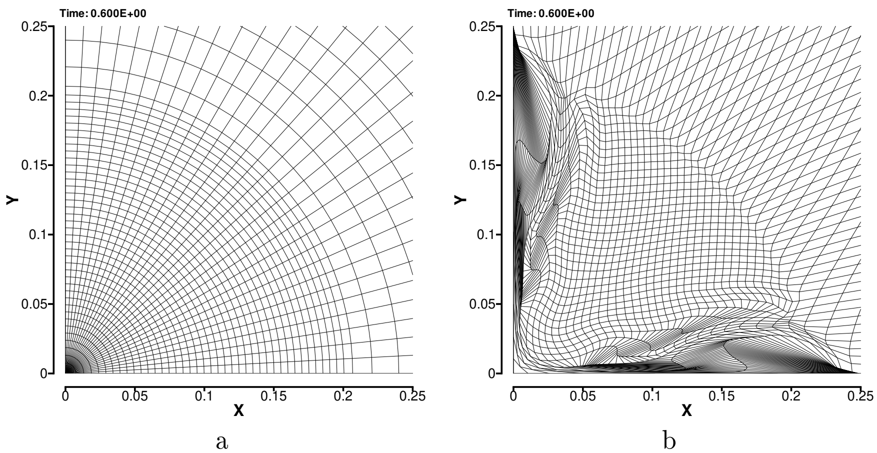

Fig. 3: Cylindrical Noh problem results for edge viscosity on a polar mesh (a) and a Cartesian mesh (b).

is negative. So Dissipativity is satisfied because the change in internal energy is proportional to $(\Delta \mathbf{v}_k)^2$, and so must be positive.

Fig. 3 shows results for the cylindrical Noh problem. The cylindrical Noh problem assumes 2D plane strain. A volume of perfect gas is given an initial unit inward radial velocity. A circular shock wave is generated from the center of convergence and propagates away from the center. At time 0.6 the analytic solution gives the shock wave a radius of 0.2. This can be seen for the polar mesh. The jets that have formed along the axes with the initially Cartesian mesh and the consequent mesh distortion are clear in the figure. Although the result shown used symmetry planes along the x and y axes the jets are not a boundary condition effect. The same results are seen if symmetry planes are not used, and the whole volume is covered by the grid.

Tensor $\mathbf{Q}$ in equation (2.1) is not a real tensor in the sense that even for smooth parameters $\mathbf{Q}$ in one zone can change dramatically. As a consequence this viscosity does not have a well defined continuum limit, which we believe causes the problems with the numerical solution shown in Fig. 3b.

3 Continuous form of tensor viscosity

3.1 Symmetric viscosity

For our new tensor viscosity we start by assuming a form similar to physical viscosity, giving a viscous stress tensor $\mathbf{Q}$ of the form

$$\mathbf{Q} = \mu \mathbf{D} \tag{3.1}$$

where μ is some scalar with the units mass/(length $\times$ time), correct for a viscosity coefficient.The possible forms of μ are constrained by the properties that we want the viscosity to satisfy. The rate of deformation tensor, $\mathbf{D}$ is defined as

$$\mathbf{D} = \frac{1}{2}(\nabla \mathbf{v} + \nabla \mathbf{v}^{\mathrm{T}}) \ . \tag{3.2}$$

For a stress tensor the momentum and energy equations are

$$\rho \frac{d\mathbf{v}}{dt} = \nabla \cdot \mathbf{Q} \quad , \quad \rho \frac{de}{dt} = \mathbf{Q} : \mathbf{D} \tag{3.3}$$

where $\mathbf{Q} : \mathbf{D} = Q_{ij} D_{ij}$ using the usual summation convention.

In order to ensure dissipativity we need to make sure that the viscosity can only decrease the kinetic energy. So in the energy equation we need to ensure that the $\mathbf{Q} : \mathbf{D}$ is always positive. With the form of $\mathbf{Q}$ in (3.1) this is easily satisfied by ensuring $\mu \geq 0$.

Self-similar motion invariance requires that $\mu = 0$ for this case, this can be achieved by including the TVD limiter function used for the edge viscosity in μ. As the tensors are held on the zone edges this is easy to do. Galilean invariance is satisfied because as the velocity field becomes constant, all terms in $\mathbf{D}$ become zero.

Viscous force continuity requires some switch to ensure that $\mu = 0$ for expansion, but this will only partly satisfy the condition, the viscosity force should also go to zero smoothly. The edge viscosity contains the term that is used to detect compression and expansion, as this term multiples all other terms in the force equation it ensures that the force does go to zero smoothly. For the tensor viscosity there is no equivalent term, so compression and expansion must be detected by a term not present in the viscosity, but this does not ensure that the viscosity will go to zero smoothly as compression vanishes. For the tensor viscosity a clear choice for defining compression and expansion is the divergence of velocity. In order to satisfy viscous force continuity a non-dimensional term would have to be added to the viscosity. For the results presented here this has not been done and so the viscosity does not fully satisfy this condition.

The final property, wave-front invariance, is satisfied because of the functional form of viscosity, so the limiter function is only required to ensure self-similar motion invariance. To check for wave front invariance we will take the case of radial flow, which was used in [6] to show wave front invariance for the edge viscosity. For 2D cylindrical coordinates (r, θ) the rate of deformation tensor is

$$\mathbf{D} = \begin{bmatrix} \dfrac{\partial v_r}{\partial r} & \dfrac{1}{2}\left(\dfrac{1}{r}\dfrac{\partial v_r}{\partial \theta} + \dfrac{\partial v_\theta}{\partial r} - \dfrac{v_\theta}{r}\right) \\ \dfrac{1}{2}\left(\dfrac{1}{r}\dfrac{\partial v_r}{\partial \theta} + \dfrac{\partial v_\theta}{\partial r} - \dfrac{v_\theta}{r}\right) & \dfrac{1}{r}\dfrac{\partial v_\theta}{\partial \theta} + \dfrac{v_r}{r} \end{bmatrix} \tag{3.4}$$

and the momentum equation is

$$\begin{aligned}
\rho a_r &= \frac{\partial Q_{rr}}{\partial r} + \frac{1}{r}\frac{\partial Q_{\theta r}}{\partial \theta} + \frac{1}{r}(Q_{rr} - Q_{\theta\theta}) \\
\rho a_\theta &= \frac{\partial Q_{r\theta}}{\partial r} + \frac{1}{r}\frac{\partial Q_{\theta\theta}}{\partial \theta} + \frac{1}{r}(Q_{r\theta} - Q_{\theta r}) \ .
\end{aligned} \tag{3.5}$$

For radial flow $v_\theta = 0$ and $\frac{\partial v_r}{\partial \theta} = 0$ so for our viscosity the momentum equation becomes

$$\begin{aligned}
\rho a_r &= \frac{\partial}{\partial r}\left(\mu \frac{\partial v_r}{\partial r}\right) + \frac{\mu}{r}\frac{\partial v_r}{\partial r} \\
\rho a_\theta &= 0 \ .
\end{aligned} \tag{3.6}$$

As the viscosity only produces accelerations in the radial direction, it satisfies the condition of wave-front invariance.

3.2 Nonsymmetric tensor viscosity

It is not necessary for an artificial viscosity to be symmetric. A nonsymmetric version of the viscosity was also developed, which starts with the gradient of velocity tensor $\mathbf{G}$ rather than the rate of deformation tensor. We define $\mathbf{Q}$ as

$$\mathbf{Q} = \mu \mathbf{G}^{\mathrm{T}} \ . \tag{3.7}$$

So the momentum and energy equations become

$$\rho \frac{d\mathbf{v}}{dt} = \nabla \cdot (\mu \mathbf{G}) \quad , \quad \rho \frac{de}{dt} = \mu \mathbf{G} : \mathbf{G} \ . \tag{3.8}$$

These equations have two useful properties for the viscosity. The first is that to satisfy the five properties the constraints on μ are the same as for the symmetric tensor. The second is that there is now no mode conversion [8]. This means that for a shear flow in which all velocities are parallel, the viscous force will only act in the velocity direction. With the symmetric tensor a force perpendicular to the velocity direction is generated.

4 Gradient of a vector and divergence of a tensor in a general coordinate system

To implement the tensor viscosity we need expressions for the divergence of a tensor and the gradient of a vector. To introduce limiters and retain good properties of the edge viscosity, it will be useful for us to write these operators using a general curvilinear coordinate system. This will allow the discrete viscosity to be held tangential to the zone edges, or normal to the median mesh. In this section we derive continuous expressions for the divergence and gradient for a

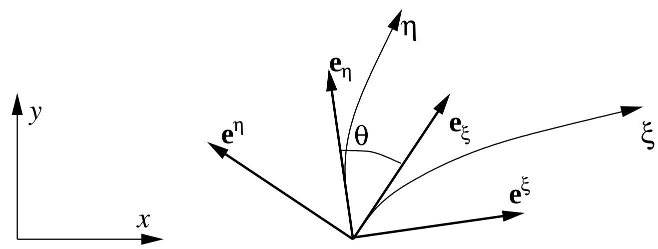

Fig. 4: Base vectors of general coordinate system (ξ, η). θ is the angle between the vectors tangential to the coordinate system.

general coordinate system. We consider the continuous case as it acts as a guide when we come to derivation of the discrete expressions.

We consider two coordinate systems, for simplicity we consider only the 2D case. The first is the standard rectangular Cartesian coordinate system, (x, y). The second is a general curvilinear system, (ξ, η), with base vectors $\mathbf{e}_\xi$ and $\mathbf{e}_\eta$ tangential to the coordinate lines, and $\mathbf{e}^\xi$ and $\mathbf{e}^\eta$ normal to the coordinate lines. These are shown in Fig. 4. The Cartesian components of the basis vectors are

$$\mathbf{e}_\xi = \begin{pmatrix} \dfrac{\partial x}{\partial \xi} \\ \\ \dfrac{\partial y}{\partial \xi} \end{pmatrix} \quad , \quad \mathbf{e}_\eta = \begin{pmatrix} \dfrac{\partial x}{\partial \eta} \\ \\ \dfrac{\partial y}{\partial \eta} \end{pmatrix} \tag{4.1}$$

It is also useful to know the metric tensor relative to the general coordinate system. The components of the metric tensor are

$$g_{\xi\xi} = \mathbf{e}_\xi \cdot \mathbf{e}_\xi \quad , \quad g_{\eta\eta} = \mathbf{e}_\eta \cdot \mathbf{e}_\eta \quad , \quad g_{\xi\eta} = g_{\eta\xi} = \mathbf{e}_\eta \cdot \mathbf{e}_\xi \quad . \tag{4.2}$$

From these the determinant of the metric tensor can be found, which we write as $|g|$.

The gradient of velocity tensor, $\mathbf{G}$, is defined as

$$\mathbf{G} = \nabla \mathbf{v} \tag{4.3}$$

or in tensor index notation

$$G_{ij} = \frac{\partial v_i}{\partial x_j} \tag{4.4}$$

where $x_1 = x$, $x_2 = y$ and $\mathbf{v} = [v_1,\ v_2] = [v_x,\ v_y]$.

4.1 Tangential projections

In the general coordinate system a tensor can be represented by two vectors which are projections to two basis vectors. Each vector is the dot product of the tensor with a unit base vector.

$$\mathbf{G}^{\xi} = \mathbf{G} \cdot \hat{\mathbf{e}}_{\xi} \quad \text{and} \quad \mathbf{G}^{\eta} = \mathbf{G} \cdot \hat{\mathbf{e}}_{\eta} \tag{4.5}$$

where the hat signifies a unit vector. Then Cartesian components of these vectors can be rewritten in terms of the derivatives of vector $\mathbf{v}$ with respect to ξ and η

$$\mathbf{G}^{\xi} = \frac{1}{\sqrt{g_{\xi\xi}}} \begin{pmatrix} \dfrac{\partial v_x}{\partial \xi} \\ \\ \dfrac{\partial v_y}{\partial \xi} \end{pmatrix} = \begin{pmatrix} \mathbf{G}^{\xi x} \\ \\ \mathbf{G}^{\xi y} \end{pmatrix} \quad , \quad \mathbf{G}^{\eta} = \frac{1}{\sqrt{g_{\eta\eta}}} \begin{pmatrix} \dfrac{\partial v_x}{\partial \eta} \\ \\ \dfrac{\partial v_y}{\partial \eta} \end{pmatrix} = \begin{pmatrix} \mathbf{G}^{\eta x} \\ \\ \mathbf{G}^{\eta y} \end{pmatrix} . \tag{4.6}$$

For future considerations in the discrete case, it is useful to derive an expression for the divergence in terms of tangential projections of a tensor using the integer identity

$$\int_V \nabla \mathbf{v} : \mathbf{T} dV = \oint_{\partial V} \mathbf{v} \cdot (\mathbf{T} \cdot \mathbf{n}) dS - \int_V \mathbf{v} \cdot (\nabla \cdot \mathbf{T}) dV \tag{4.7}$$

where $\mathbf{T}$ is any second order tensor. $\nabla \mathbf{v} : \mathbf{T}$ is the scalar product of two tensors, which in a Cartesian coordinate system is

$$\mathbf{G} : \mathbf{T} = G_{ij} T_{ij} \ . \tag{4.8}$$

For tensors a second scalar product is also possible, this is written

$$\mathbf{G} \cdot \cdot \mathbf{T} = G_{ij} T_{ji} \ . \tag{4.9}$$

To use the identity an expression for the scalar product in terms of the tangential projections is required. The scalar product is defined in terms of the Cartesian components of the two tensors, so we start by defining the Cartesian components of $\mathbf{G}$ in terms of $\mathbf{G}^{\xi}$ and $\mathbf{G}^{\eta}$. These formulae are valid for any tensor, and are found by solving the set of equations represented by equation (4.5)

$$\begin{aligned} G_{xx} &= \frac{\sqrt{g_{\xi\xi}}}{\sqrt{|g|}} \frac{\partial y}{\partial \eta} \mathbf{G}^{\xi x} - \frac{\sqrt{g_{\eta\eta}}}{\sqrt{|g|}} \frac{\partial y}{\partial \xi} \mathbf{G}^{\eta x} \\ G_{xy} &= \frac{\sqrt{g_{\eta\eta}}}{\sqrt{|g|}} \frac{\partial x}{\partial \xi} \mathbf{G}^{\eta x} - \frac{\sqrt{g_{\xi\xi}}}{\sqrt{|g|}} \frac{\partial x}{\partial \eta} \mathbf{G}^{\xi x} \\ G_{yx} &= \frac{\sqrt{g_{\xi\xi}}}{\sqrt{|g|}} \frac{\partial y}{\partial \eta} \mathbf{G}^{\xi y} - \frac{\sqrt{g_{\eta\eta}}}{\sqrt{|g|}} \frac{\partial y}{\partial \xi} \mathbf{G}^{\eta y} \\ G_{yy} &= \frac{\sqrt{g_{\eta\eta}}}{\sqrt{|g|}} \frac{\partial x}{\partial \xi} \mathbf{G}^{\eta y} - \frac{\sqrt{g_{\xi\xi}}}{\sqrt{|g|}} \frac{\partial x}{\partial \eta} \mathbf{G}^{\xi y} \ . \end{aligned} \tag{4.10}$$

Now it is possible to write down the scalar product and collect terms to get

$$\begin{aligned} \mathbf{G} : \mathbf{T} \quad = \quad & \mathbf{G}^{\xi} \cdot \left[\mathbf{T}^{\xi} \frac{g_{\xi\xi} g_{\eta\eta}}{|g|} - \mathbf{T}^{\eta} \frac{g_{\xi\eta}}{|g|} \sqrt{g_{\xi\xi}} \sqrt{g_{\eta\eta}} \right] + \\ & \mathbf{G}^{\eta} \cdot \left[\mathbf{T}^{\eta} \frac{g_{\xi\xi} g_{\eta\eta}}{|g|} - \mathbf{T}^{\xi} \frac{g_{\xi\eta}}{|g|} \sqrt{g_{\xi\xi}} \sqrt{g_{\eta\eta}} \right] . \end{aligned} \tag{4.11}$$

Rearranging and noting that

$$\frac{g_{\xi\xi}g_{\eta\eta}}{|g|} = \frac{1}{\sin^2\theta} \quad , \quad \frac{g_{\xi\eta}}{\sqrt{g_{\xi\xi}}\sqrt{g_{\eta\eta}}} = \cos\theta \tag{4.12}$$

allows the scalar product to be written only in terms of the tangential projections and the angle θ between $\mathbf{e}_\xi$ and $\mathbf{e}_\eta$, Fig 4.

$$\mathbf{G}:\mathbf{T} \quad = \quad \frac{1}{\sin^2\theta}\left[\mathbf{G}^\xi\cdot\mathbf{T}^\xi + \mathbf{G}^\eta\cdot\mathbf{T}^\eta - \cos\theta(\mathbf{G}^\xi\cdot\mathbf{T}^\eta + \mathbf{G}^\eta\cdot\mathbf{T}^\xi)\right]. \tag{4.13}$$

Comparing (4.13) to the expression for the vector dot product in [9] shows that the two expressions are equivalent except that the ξ and η terms are vectors in our case.

In deriving an expression for the divergence using the identity in (4.7) we assume, for simplicity, that the surface integral is zero. Then use equation (4.11) for $\nabla\mathbf{v}:\mathbf{T}$ and replace the $\mathbf{G}^\xi$ and $\mathbf{G}^\eta$ terms with the derivatives of vector $\mathbf{v}$ using (4.6). This gives

$$\begin{aligned}\iint \nabla\mathbf{v}:\mathbf{T}\sqrt{|g|}d\xi d\eta \quad &= \iint \Bigg(\quad \frac{\partial\mathbf{v}}{\partial\xi}\cdot\left[\frac{\mathbf{T}^\xi - \cos\theta\mathbf{T}^\eta}{\sqrt{g_{\xi\xi}}\sin^2\theta}\right] + \\ &\qquad\qquad \frac{\partial\mathbf{v}}{\partial\eta}\cdot\left[\frac{\mathbf{T}^\eta - \cos\theta\mathbf{T}^\xi}{\sqrt{g_{\eta\eta}}\sin^2\theta}\right]\Bigg)\sqrt{|g|}d\xi d\eta \ .\end{aligned} \tag{4.14}$$

Integrating this expression by parts gives two terms that are equivalent to the RHS of equation (4.7). Ignoring the terms representing the surface integral leaves

$$\begin{aligned}\iint \mathbf{v}\cdot(\nabla\cdot\mathbf{T})\sqrt{|g|}d\xi d\eta \quad &= \iint \Bigg(\quad \mathbf{v}\cdot\frac{\partial}{\partial\xi}\left[\sqrt{|g|}\frac{\mathbf{T}^\xi - \cos\theta\mathbf{T}^\eta}{\sqrt{g_{\xi\xi}}\sin^2\theta}\right] + \\ &\qquad\qquad \mathbf{v}\cdot\frac{\partial}{\partial\eta}\left[\sqrt{|g|}\frac{\mathbf{T}^\eta - \cos\theta\mathbf{T}^\xi}{\sqrt{g_{\eta\eta}}\sin^2\theta}\right]\Bigg)d\xi d\eta \ .\end{aligned} \tag{4.15}$$

Now we can write the expression for the divergence

$$\begin{aligned}\nabla\cdot\mathbf{T} \quad &= \frac{1}{\sqrt{|g|}}\Bigg\{ \quad \frac{\partial}{\partial\xi}\left[\sqrt{|g|}\frac{\mathbf{T}^\xi - \cos\theta\mathbf{T}^\eta}{\sqrt{g_{\xi\xi}}\sin^2\theta}\right] + \\ &\qquad\qquad \frac{\partial}{\partial\eta}\left[\sqrt{|g|}\frac{\mathbf{T}^\eta - \cos\theta\mathbf{T}^\xi}{\sqrt{g_{\eta\eta}}\sin^2\theta}\right]\Bigg\}.\end{aligned} \tag{4.16}$$

This can also be derived directly from the expression for the divergence in terms of T_{xx}, T_{yy} and T_{xy}. However from a methodological point of view it is useful to derive it using the integral identity.

4.2 Normal projections

Instead of using tangential projections it is possible to use normal projections. A tensor is again written as two vectors, each vector is the dot product of the tensor with a unit vector normal to a curvilinear coordinate axis, Fig 4.

$$\mathbf{G}_\xi = \mathbf{G} \cdot \hat{\mathbf{e}}^\xi \quad \text{and} \quad \mathbf{G}_\eta = \mathbf{G} \cdot \hat{\mathbf{e}}^\eta. \tag{4.17}$$

These can then be solved to get

$$\begin{aligned}
G_{xx} &= \frac{\sqrt{g_{\eta\eta}}}{\sqrt{|g|}} \frac{\partial x}{\partial \xi} \mathbf{G}_{\xi x} + \frac{\sqrt{g_{\xi\xi}}}{\sqrt{|g|}} \frac{\partial x}{\partial \eta} \mathbf{G}_{\eta x} \\
G_{xy} &= \frac{\sqrt{g_{\xi\xi}}}{\sqrt{|g|}} \frac{\partial y}{\partial \eta} \mathbf{G}_{\eta x} + \frac{\sqrt{g_{\eta\eta}}}{\sqrt{|g|}} \frac{\partial y}{\partial \xi} \mathbf{G}_{\xi x} \\
G_{yx} &= \frac{\sqrt{g_{\eta\eta}}}{\sqrt{|g|}} \frac{\partial x}{\partial \xi} \mathbf{G}_{\xi y} + \frac{\sqrt{g_{\xi\xi}}}{\sqrt{|g|}} \frac{\partial x}{\partial \eta} \mathbf{G}_{\eta y} \\
G_{yy} &= \frac{\sqrt{g_{\xi\xi}}}{\sqrt{|g|}} \frac{\partial y}{\partial \eta} \mathbf{G}_{\eta y} + \frac{\sqrt{g_{\eta\eta}}}{\sqrt{|g|}} \frac{\partial y}{\partial \xi} \mathbf{G}_{\xi y} \ .
\end{aligned} \tag{4.18}$$

Following the same method used for the tangential projections gives an expression for the scalar product

$$\mathbf{G} : \mathbf{T} \quad = \quad \frac{1}{\sin^2\theta} \left[\mathbf{G}_\xi \cdot \mathbf{T}_\xi + \mathbf{G}_\eta \cdot \mathbf{T}_\eta + \cos\theta (\mathbf{G}_\xi \cdot \mathbf{T}_\eta + \mathbf{G}_\eta \cdot \mathbf{T}_\xi) \right]. \tag{4.19}$$

When using normal projections it is most convenient to start with the divergence and derive the gradient. The divergence in terms of the normal projections is derived by substituting (4.18) into the the definition of divergence in Cartesian components. This gives

$$\nabla \cdot \mathbf{T} = \frac{1}{\sqrt{|g|}} \left\{ \frac{\partial}{\partial \xi} \left[\sqrt{g_{\eta\eta}} \mathbf{T}_\xi \right] + \frac{\partial}{\partial \eta} \left[\sqrt{g_{\xi\xi}} \mathbf{T}_\eta \right] \right\}. \tag{4.20}$$

Now to derive an expression for the gradient, substitute (4.20) into the integral identity (4.7). Then ignoring the terms representing the surface integral will leave

$$\nabla \mathbf{v} : \mathbf{T} = \frac{1}{\sqrt{|g|}} \left\{ \mathbf{T}_\xi \sqrt{g_{\eta\eta}} \frac{\partial \mathbf{v}}{\partial \xi} + \mathbf{T}_\eta \sqrt{g_{\xi\xi}} \frac{\partial \mathbf{v}}{\partial \eta} \right\}. \tag{4.21}$$

Equating (4.21) with (4.19) allows the gradient to be written in terms of $\mathbf{G}_\xi$ and $\mathbf{G}_\eta$

$$\begin{aligned}
\frac{\partial \mathbf{v}}{\partial \xi} \quad &= \quad \frac{\sqrt{|g|}}{\sqrt{g_{\eta\eta}} \sin^2\theta} (\mathbf{G}_\xi + \cos\theta \mathbf{G}_\eta) \\
\frac{\partial \mathbf{v}}{\partial \eta} \quad &= \quad \frac{\sqrt{|g|}}{\sqrt{g_{\xi\xi}} \sin^2\theta} (\cos\theta \mathbf{G}_\xi + \mathbf{G}_\eta) \ .
\end{aligned} \tag{4.22}$$

Then solving this set of equations gives expressions for $\mathbf{G}_\xi$ and $\mathbf{G}_\eta$ in terms of the directional derivatives of the velocity

$$\begin{aligned} \mathbf{G}_\xi &= \frac{1}{\sqrt{|g|}} \left\{ \sqrt{g_{\eta\eta}} \frac{\partial \mathbf{v}}{\partial \xi} - \sqrt{g_{\xi\xi}} \cos\theta \frac{\partial \mathbf{v}}{\partial \eta} \right\} \\ \mathbf{G}_\eta &= \frac{1}{\sqrt{|g|}} \left\{ -\sqrt{g_{\eta\eta}} \cos\theta \frac{\partial \mathbf{v}}{\partial \xi} + \sqrt{g_{\xi\xi}} \frac{\partial \mathbf{v}}{\partial \eta} \right\}. \end{aligned} \tag{4.23}$$

5 Discrete tensor operators

This section describes the derivation of discrete forms of the gradient of a vector and divergence of a tensor on a logically rectangular grid. Two different derivations are shown, both have separately been used for the artificial viscosity. Both derivations use the support-operator method (SOM) [10, 11, 12]. In the SOM a discrete approximation for a differential operator, such as divergence or gradient, is chosen. This initial or prime operator then supports the derivation of other discrete operators.

The first derivation uses tangential projections on zone edges and is an extension of the SOM for general grids [13, 14, 9] to second order tensors. The second derivation uses normal projections on the median mesh. This calculates the gradient of velocity in the same subzone volume used by the edge viscosity.

5.1 Grid

We use a logically rectangular grid to construct the discrete functions. The nodes of the grid are labelled using (i,j), where $1 \le i \le M$ and $1 \le j \le N$. The zone defined by the four nodes (i,j), $(i+1,j)$, $(i+1,j+1)$ and $(i,j+1)$ is called $(i+\frac{1}{2}, j+\frac{1}{2})$. The zone edge between the nodes (i,j) and $(i+1,j)$ is called $(i+\frac{1}{2}, j)$, and the edge between nodes (i,j) and $(i,j+1)$ is called $(i, j+\frac{1}{2})$.

It is convenient to think of the zone edges as approximations to the coordinate curves of the general coordinate system (ξ,η). The ξ coordinate curve corresponds to the grid line where i is changing, the η coordinate curve to the line where j is changing.

We denote the length of edge $(i+\frac{1}{2}, j)$ as $l\xi_{i+\frac{1}{2},j}$, and the length of edge $(i, j+\frac{1}{2})$ as $l\eta_{i,j+\frac{1}{2}}$. The area of zone $(i+\frac{1}{2}, j+\frac{1}{2})$ is $V_{i+\frac{1}{2},j+\frac{1}{2}}$. The angle between two edges of zone $(i+\frac{1}{2}, j+\frac{1}{2})$ that meet at node (k,l) is denoted $\theta_{k,l}^{i+\frac{1}{2},j+\frac{1}{2}}$, see Fig. 5. The same subscript and superscript are used to denote any value that is held at a node and associated with one of the four adjacent zones. The nodal area $V_{i,j}$ is the area of the octagon defined by the median mesh surrounding node (i,j).

As each edge is adjacent to two sections of the median mesh is is necessary to label the vectors normal to the median mesh with both edge and zone information, so $\mathbf{s}_{i+\frac{1}{2},j}^{i+\frac{1}{2},j+\frac{1}{2}}$ is the normal vector to the section of the median mesh that connects the center of zone $(i+\frac{1}{2}, j+\frac{1}{2})$ to the center of edge $(i+\frac{1}{2}, j)$.

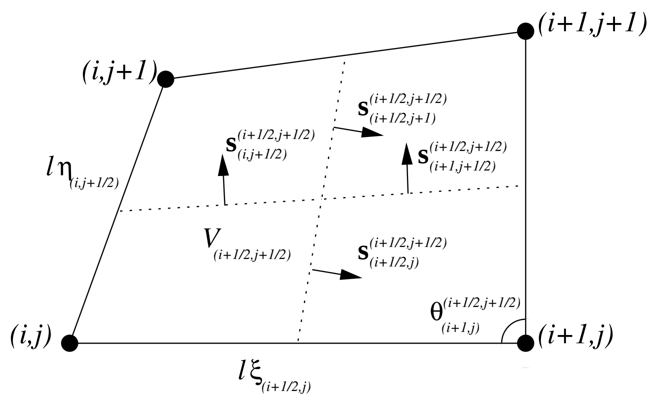

Fig. 5: Typical zone of logically rectangular grid. The solid lines are the zone edges, the dotted line the median mesh.

On the grid there are four locations where we can choose to hold values of a discrete function, these are the nodes, the zone centers, the zone edges and the median mesh edges. Here we will only consider the case where scalars are held at the zone centers, vectors at the nodes and tensors at zone edges as projections parallel to the edge, or normal to the edges of the median mesh.

The space of zone centered discrete scalar functions is labelled HC, the notation $a_{i+\frac{1}{2},j+\frac{1}{2}}$ is used for the values of scalar function a. The space of nodal discrete vector functions is labelled $\mathcal{HN}$, the notation $v_{x(i,j)}$ and $v_{y(i,j)}$ is used for the components of vector $\mathbf{v}$. The space of tensor functions held as tangential projections on an edge is labelled $\widehat{\mathcal{HL}}$, the notation $\mathbf{T}^{\xi}_{i+\frac{1}{2},j}$ and $\mathbf{T}^{\eta}_{i,j+\frac{1}{2}}$ is used for the vector components formed by the tangential projection of tensor $\mathbf{T}$ to the zone edges. The space of tensor functions held as normal projections on the median mesh is labelled $\widehat{\mathcal{HS}}$.

5.2 Derivation of discrete operators for edge tangential projections

5.2.1 The prime operator

With edge tangential projections we need to know the following two operators

$$\mathbf{GRAD} : \mathcal{HN} \to \widehat{\mathcal{HL}} \tag{5.1}$$

$$\mathbf{DIV} : \widehat{\mathcal{HL}} \to \mathcal{HN} \tag{5.2}$$

GRAD is the discrete form of the vector gradient, **DIV** the discrete form of the tensor divergence. To use the SOM we must choose one of these two operators as the prime operator. As **GRAD** is easily defined for such discrete spaces we choose it as the prime operator.

For a given direction l, given by unit vector $\mathbf{l}$, the directional derivative of vector field $\mathbf{v}$ is:

$$\frac{\partial \mathbf{v}}{\partial l} = \mathbf{l} \cdot \nabla \mathbf{v} \ . \tag{5.3}$$

This leads to the definition of the projections of tensor $\mathbf{G} = \mathbf{GRAD}\ \mathbf{v}$ as

$$\mathbf{G}^{\xi}_{i+\frac{1}{2},j} = \frac{\mathbf{v}_{i+1,j} - \mathbf{v}_{i,j}}{l\xi_{i+\frac{1}{2},j}} \quad , \quad \mathbf{G}^{\eta}_{i,j+\frac{1}{2}} = \frac{\mathbf{v}_{i,j+1} - \mathbf{v}_{i,j}}{l\eta_{i,j+\frac{1}{2}}} \ . \tag{5.4}$$

The agreement between equations (5.4) and (4.6) is clear when we recall the identities

$$dl_{\xi} = \sqrt{g_{\xi\xi}}d\xi \quad , \quad dl_{\eta} = \sqrt{g_{\eta\eta}}d\eta \tag{5.5}$$

where dl_{ξ} and dl_{η} are the elements of arcs of coordinate curves.

5.2.2 The derived operator

We now use the prime operator **GRAD** to support the derivation of the discrete operator

$$\mathbf{DIV} : \widehat{\mathcal{HL}} \rightarrow \mathcal{HN} \tag{5.6}$$

as the negative adjoint of **GRAD**.

The first step is to get a discrete form of equation (4.13), the tensor scalar product. We approximate the continuous equation by

$$\begin{aligned}(\mathbf{G},\mathbf{T})_{i+\frac{1}{2},j+\frac{1}{2}} = \sum_{k,l=0}^{1} & \frac{V^{i+\frac{1}{2},j+\frac{1}{2}}_{i+k,j+l}}{\sin^2 \theta^{i+\frac{1}{2},j+\frac{1}{2}}_{i+k,j+l}} \Big\{ \\ & \mathbf{G}^{\xi}_{i+\frac{1}{2},j+l} \cdot \mathbf{T}^{\xi}_{i+\frac{1}{2},j+l} + \mathbf{G}^{\eta}_{i+k,j+\frac{1}{2}} \cdot \mathbf{T}^{\eta}_{i+k,j+\frac{1}{2}} + \\ & (-1)^{k+l} \cos \theta^{i+\frac{1}{2},j+\frac{1}{2}}_{i+k,j+l} \big[\\ & \mathbf{G}^{\xi}_{i+\frac{1}{2},j+l} \cdot \mathbf{T}^{\eta}_{i+k,j+\frac{1}{2}} + \mathbf{G}^{\eta}_{i+k,j+\frac{1}{2}} \cdot \mathbf{T}^{\xi}_{i+\frac{1}{2},j+l} \big] \Big\}\end{aligned} \tag{5.7}$$

which gives the scalar product evaluated at the center of zone $(i + \frac{1}{2}, j + \frac{1}{2})$. $V^{i+\frac{1}{2},j+\frac{1}{2}}_{i+k,j+l}$ are some weights that satisfy

$$V^{i+\frac{1}{2},j+\frac{1}{2}}_{i+k,j+l} \geq 0 \quad , \quad \sum_{k,l=0}^{1} V^{i+\frac{1}{2},j+\frac{1}{2}}_{i+k,j+l} = 1 \ . \tag{5.8}$$

We define $V^{i+\frac{1}{2},j+\frac{1}{2}}_{i+k,j+l}$ as one half of the area of the triangle in zone $(i + \frac{1}{2}, j + \frac{1}{2})$ which contains the angle at node $(i + k, j + l)$, divided by the volume of the zone. This choice of weights gives a first order approximation of the operator [13].

To derive **DIV** from (5.7) and (5.4) we use the discrete form of the integral identity (4.7) and assume for simplicity that the surface integral is zero. This gives us

$$\sum_{i=1}^{M-1}\sum_{j=1}^{N-1}(\mathbf{G},\mathbf{T})_{i+\frac{1}{2},j+\frac{1}{2}}V_{i+\frac{1}{2},j+\frac{1}{2}} = -\sum_{i=1}^{M}\sum_{j=1}^{N}(\mathbf{v},\mathbf{DIV}\ \mathbf{T})_{i,j}V_{i,j}\ . \tag{5.9}$$

Substitute (5.7) into (5.9) and collect the $\mathbf{G}^{\xi}$ and $\mathbf{G}^{\eta}$ terms. For a zone each of these terms is known in two locations, the ξ terms are known on the $(i+\frac{1}{2},j)$ and $(i+\frac{1}{2},j+1)$ edges and the η terms on the $(i,j+\frac{1}{2})$ and $(i+1,j+\frac{1}{2})$ edges. By changing the limits on the sums the equation can be rewritten such that only $\mathbf{G}^{\xi}_{i+\frac{1}{2},j}$ and $\mathbf{G}^{\eta}_{i,j+\frac{1}{2}}$ appear. So for example

$$\sum_{i=1}^{M-1}\sum_{j=1}^{N-1}\frac{\cos\theta^{i+\frac{1}{2},j+\frac{1}{2}}_{i+1,j+1}}{\sin^2\theta^{i+\frac{1}{2},j+\frac{1}{2}}_{i+1,j+1}}\mathbf{G}^{\xi}_{i+\frac{1}{2},j+1}\cdot\mathbf{T}^{\eta}_{i+1,j+\frac{1}{2}}$$

becomes

$$\sum_{i=1}^{M-1}\sum_{j=2}^{N}\frac{\cos\theta^{i+\frac{1}{2},j-\frac{1}{2}}_{i+1,j}}{\sin^2\theta^{i+\frac{1}{2},j-\frac{1}{2}}_{i+1,j}}\mathbf{G}^{\xi}_{i+\frac{1}{2},j}\cdot\mathbf{T}^{\eta}_{i+1,j-\frac{1}{2}}\ .$$

This gives an equation of the form

$$\sum_{i=1}^{M-1}\sum_{j=1}^{N-1}\mathbf{G}^{\xi}_{i+\frac{1}{2},j}\cdot f(\mathbf{T},\theta)+\sum_{i=1}^{M-1}\sum_{j=2}^{N}\mathbf{G}^{\xi}_{i+\frac{1}{2},j}\cdot f(\mathbf{T},\theta)+(\mathbf{G}^{\eta}\text{ terms})\ .$$

Next substitute for $\mathbf{G}^{\xi}$ and $\mathbf{G}^{\eta}$ using (5.4) to get an equation containing the components of vector $\mathbf{v}$. The equation will contain $\mathbf{v}$ terms at three locations, the nodes (i,j), $(i+1,j)$ and $(i,j+1)$. Again rewrite the equations to collect all the $\mathbf{v}$ terms at (i,j) using the same method described above. This expression can then be equated to the RHS of (5.9) to get an expression for $(\mathbf{DIV}\ \mathbf{T})_{i,j}$.

$$\begin{aligned}(\mathbf{DIV}\ \mathbf{T})_{i,j} &= \frac{1}{V_{i,j}}\Bigg\{\ \frac{(L_{11}\mathbf{T}^{\xi}+L_{12}\mathbf{T}^{\eta})_{i+\frac{1}{2},j}}{l\xi_{i+\frac{1}{2},j}}-\\ &\qquad\frac{(L_{11}\mathbf{T}^{\xi}+L_{12}\mathbf{T}^{\eta})_{i-\frac{1}{2},j}}{l\xi_{i-\frac{1}{2},j}}+\\ &\qquad\frac{(L_{21}\mathbf{T}^{\xi}+L_{22}\mathbf{T}^{\eta})_{i,j+\frac{1}{2}}}{l\eta_{i,j+\frac{1}{2}}}-\\ &\qquad\frac{(L_{21}\mathbf{T}^{\xi}+L_{22}\mathbf{T}^{\eta})_{i,j-\frac{1}{2}}}{l\eta_{i,j-\frac{1}{2}}}\Bigg\}\end{aligned} \tag{5.10}$$

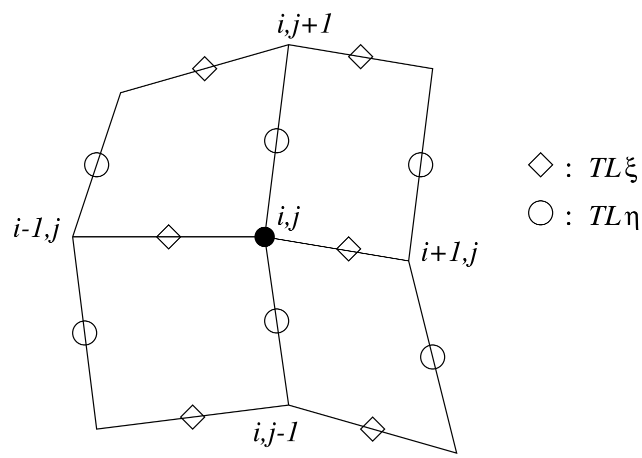

Fig. 6: Stencil for operator $(\mathbf{DIV\ T})_{(i,j)}$

where

$$
\begin{aligned}
(L_{11}\mathbf{T}^{\xi})_{i+\frac{1}{2},j} &= \mathbf{T}^{\xi}_{i+\frac{1}{2},j}\sum_{k,l=0}^{1}\left(\frac{V}{\sin^2\theta}\right)_{i+k,j}^{i+\frac{1}{2},j+l-\frac{1}{2}} \\
(L_{12}\mathbf{T}^{\eta})_{i+\frac{1}{2},j} &= -\sum_{k,l=0}^{1}(-1)^{k+l}\left(\frac{V\cos\theta}{\sin^2\theta}\right)_{i+k,j}^{i+\frac{1}{2},j+l-\frac{1}{2}}\mathbf{T}^{\eta}_{i+k,j+l-\frac{1}{2}} \\
(L_{21}\mathbf{T}^{\xi})_{i,j+\frac{1}{2}} &= -\sum_{k,l=0}^{1}(-1)^{k+l}\left(\frac{V\cos\theta}{\sin^2\theta}\right)_{i,j+l}^{i+k-\frac{1}{2},j+\frac{1}{2}}\mathbf{T}^{\xi}_{i+k-\frac{1}{2},j+l} \\
(L_{22}\mathbf{T}^{\eta})_{i,j+\frac{1}{2}} &= \mathbf{T}^{\eta}_{i,j+\frac{1}{2}}\sum_{k,l=0}^{1}\left(\frac{V}{\sin^2\theta}\right)_{i,j+l}^{i+k-\frac{1}{2},j+\frac{1}{2}}.
\end{aligned}
\tag{5.11}
$$

The stencil for operator $(\mathbf{DIV\ T})_{i,j}$ is shown in Fig. 6.

On the boundary, any term whose index lies outside the body is taken to be zero. The L_{11}, L_{12}, L_{21} and L_{22} operators are the same as for the approximation for the divergence of a vector derived in [9].

It is interesting to note that it is now possible to use this expression to derive an approximation to the gradient of a scalar when the scalar is known at the zone edges. This is done by substituting $\mathbf{T} = \phi\mathbf{I}$, where ϕ is a scalar and $\mathbf{I}$ is the identity tensor, into (5.10). The approximations for gradient of a scalar derived in [14, 9] are only for a scalar held at a zone center or node.

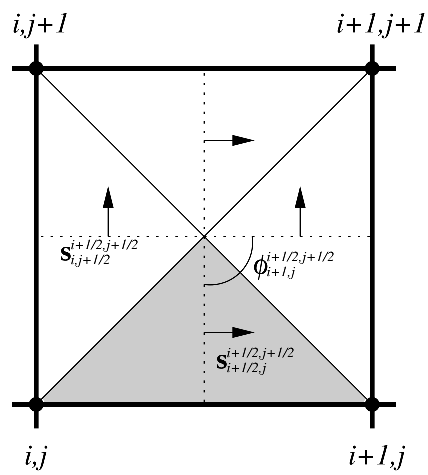

Fig. 7: Zone $i+\frac{1}{2}, j+\frac{1}{2}$. The solid lines show the boundaries of the triangular subzones, one subzone is shaded. The dotted lines show the median mesh. The vectors normal to the median mesh, $\mathbf{s}$, are defined as positive in the direction shown.

5.3 Derivation of discrete operators for median normal projections

For median normal projections we need to know the following two operators

$$\mathbf{GRAD} : \mathcal{HN} \rightarrow \widehat{\mathcal{HS}} \tag{5.12}$$

$$\mathbf{DIV} : \widehat{\mathcal{HS}} \rightarrow \mathcal{HN} \tag{5.13}$$

5.3.1 The prime operator

When the tensor is known in terms of its normal projections to the median mesh, divergence is the clear choice of prime operator. We define divergence of a tensor at a node in the common finite difference form of a surface integral on the median mesh around the node.

Here we allow the tensor to vary inside a zone, but constrain it saying that it must be constant along each segment of the median mesh. This is equivalent to defining the tensor as constant inside the triangular subzone volumes used by the edge viscosity, Fig. 7.

The divergence of $\mathbf{T}$ for a node is

$$\begin{aligned}(\mathbf{DIV}\ \mathbf{T})_{i,j} \;=\; \Big[& (\mathbf{T}_\eta|\mathbf{s}|)_{i+\frac{1}{2},j}^{i+\frac{1}{2},j+\frac{1}{2}} + (\mathbf{T}_\xi|\mathbf{s}|)_{i,j+\frac{1}{2}}^{i+\frac{1}{2},j+\frac{1}{2}} + (\mathbf{T}_\xi|\mathbf{s}|)_{i,j+\frac{1}{2}}^{i-\frac{1}{2},j+\frac{1}{2}} \\ & -(\mathbf{T}_\eta|\mathbf{s}|)_{i-\frac{1}{2},j}^{i-\frac{1}{2},j+\frac{1}{2}} - (\mathbf{T}_\eta|\mathbf{s}|)_{i-\frac{1}{2},j}^{i-\frac{1}{2},j-\frac{1}{2}} - (\mathbf{T}_\xi|\mathbf{s}|)_{i,j-\frac{1}{2}}^{i-\frac{1}{2},j-\frac{1}{2}} \\ & -(\mathbf{T}_\xi|\mathbf{s}|)_{i,j-\frac{1}{2}}^{i+\frac{1}{2},j-\frac{1}{2}} + (\mathbf{T}_\eta|\mathbf{s}|)_{i+\frac{1}{2},j}^{i+\frac{1}{2},j-\frac{1}{2}} \Big] / V_{i,j}\end{aligned} \tag{5.14}$$

$|\mathbf{s}|$ means the length of $\mathbf{s}$. $(\mathbf{T}_\eta|\mathbf{s}|)^{i+\frac{1}{2},j+\frac{1}{2}}_{i+\frac{1}{2},j}$ denotes the value from the subzone in zone $(i+\frac{1}{2},j+\frac{1}{2})$ adjacent to edge $(i+\frac{1}{2},j)$.

5.3.2 The derived operator

From equation (5.14) it is easy to get an expression for $(\mathbf{v},\mathbf{DIV}\ \mathbf{T})_{i,j}$. From this an expression for $(\mathbf{G},\mathbf{T})_{i+\frac{1}{2},j+\frac{1}{2}}$ can be found by using the discrete form of the integral identity (5.9)

$$
\begin{aligned}
(\mathbf{G},\mathbf{T})_{i+\frac{1}{2},j+\frac{1}{2}} \quad = \quad & \Big[\ \mathbf{T}_{\eta}{}^{i+\frac{1}{2},j+\frac{1}{2}}_{i+\frac{1}{2},j}\cdot(\mathbf{v}_{i+1,j}-\mathbf{v}_{i,j})|\mathbf{s}|^{i+\frac{1}{2},j+\frac{1}{2}}_{i+\frac{1}{2},j} \\
& +\mathbf{T}_{\eta}{}^{i+\frac{1}{2},j+\frac{1}{2}}_{i+\frac{1}{2},j+1}\cdot(\mathbf{v}_{i+1,j+1}-\mathbf{v}_{i,j+1})|\mathbf{s}|^{i+\frac{1}{2},j+\frac{1}{2}}_{i+\frac{1}{2},j+1} \\
& +\mathbf{T}_{\xi}{}^{i+\frac{1}{2},j+\frac{1}{2}}_{i,j+\frac{1}{2}}\cdot(\mathbf{v}_{i,j+1}-\mathbf{v}_{i,j})|\mathbf{s}|^{i+\frac{1}{2},j+\frac{1}{2}}_{i,j+\frac{1}{2}} \\
& +\mathbf{T}_{\xi}|\mathbf{s}|^{i+\frac{1}{2},j+\frac{1}{2}}_{i+1,j+\frac{1}{2}}\cdot(\mathbf{v}_{i+1,j+1}-\mathbf{v}_{i+1,j})|\mathbf{s}|^{i+\frac{1}{2},j+\frac{1}{2}}_{i+1,j+\frac{1}{2}}\Big]/V_{i+\frac{1}{2},j+\frac{1}{2}}\ .
\end{aligned} \tag{5.15}
$$

Following the same method used to derive the divergence for the tangential projections the next step is to gather all the $\mathbf{T}$ terms at one location in the grid. However as there are both $\mathbf{T}_\xi$ and $\mathbf{T}_\eta$ terms and we are not assuming that $\mathbf{T}$ is constant in a zone this is next step is not possible.

To use equation (5.14) it is not necessary to know the full tensor in each subzone, only the projection. For the general form of viscosity stress tensor we have assumed, calculating the projection of the stress tensor only requires knowledge of the projection of the velocity gradient tensor. So it is only necessary to calculate $\mathbf{G}_\xi$ and $\mathbf{G}_\eta$. To do this we start with an alternative expression for the tensor scalar product in a zone,

$$
\begin{aligned}
(\mathbf{G},\mathbf{T})_{i+\frac{1}{2},j+\frac{1}{2}} = \quad & \sum_{k,l=0}^{1}\frac{V^{i+\frac{1}{2},j+\frac{1}{2}}_{i+k,j+l}}{\sin^2\phi^{i+\frac{1}{2},j+\frac{1}{2}}_{i+k,j+l}}\Big\{ \\
& \quad \mathbf{G}_{\eta}{}^{i+\frac{1}{2},j+\frac{1}{2}}_{i+\frac{1}{2},j+1}\cdot\mathbf{T}_{\eta}{}^{i+\frac{1}{2},j+\frac{1}{2}}_{i+\frac{1}{2},j+l}+\mathbf{G}_{\xi}{}^{i+\frac{1}{2},j+\frac{1}{2}}_{i+k,j+\frac{1}{2}}\cdot\mathbf{T}_{\xi}{}^{i+\frac{1}{2},j+\frac{1}{2}}_{i+k,j+\frac{1}{2}}- \\
& (-1)^{k+l}\cos\phi^{i+\frac{1}{2},j+\frac{1}{2}}_{i+k,j+l}\big[\\
& \quad \mathbf{G}_{\eta}{}^{i+\frac{1}{2},j+\frac{1}{2}}_{i+\frac{1}{2},j+1}\cdot\mathbf{T}_{\xi}{}^{i+\frac{1}{2},j+\frac{1}{2}}_{i+k,j+\frac{1}{2}}+\mathbf{G}_{\xi}{}^{i+\frac{1}{2},j+\frac{1}{2}}_{i+k,j+\frac{1}{2}}\cdot\mathbf{T}_{\eta}{}^{i+\frac{1}{2},j+\frac{1}{2}}_{i+\frac{1}{2},j+1}\big]\Big\}.
\end{aligned} \tag{5.16}
$$

This is the discrete version of the tensor scalar product in terms of normal projections, equation (4.19). This equation can be rearranged to give terms like

$$
\begin{aligned}
\mathbf{T}_{\eta}{}^{i+\frac{1}{2},j+\frac{1}{2}}_{i+\frac{1}{2},j}\Bigg[& \frac{V^{i+\frac{1}{2},j+\frac{1}{2}}_{i,j}}{\sin^2\phi^{i+\frac{1}{2},j+\frac{1}{2}}_{i,j}}\left\{\mathbf{G}_{\eta}{}^{i+\frac{1}{2},j+\frac{1}{2}}_{i+\frac{1}{2},j}-\cos\phi^{i+\frac{1}{2},j+\frac{1}{2}}_{i,j}\mathbf{G}_{\xi}{}^{i+\frac{1}{2},j+\frac{1}{2}}_{i,j+\frac{1}{2}}\right\} \\
& +\frac{V^{i+\frac{1}{2},j+\frac{1}{2}}_{i+1,j}}{\sin^2\phi^{i+\frac{1}{2},j+\frac{1}{2}}_{i+1,j}}\left\{\mathbf{G}_{\eta}{}^{i+\frac{1}{2},j+\frac{1}{2}}_{i+\frac{1}{2},j}+\cos\phi^{i+\frac{1}{2},j+\frac{1}{2}}_{i+1,j}\mathbf{G}_{\xi}{}^{i+\frac{1}{2},j+\frac{1}{2}}_{i+1,j+\frac{1}{2}}\right\}\Bigg]
\end{aligned} \tag{5.17}
$$

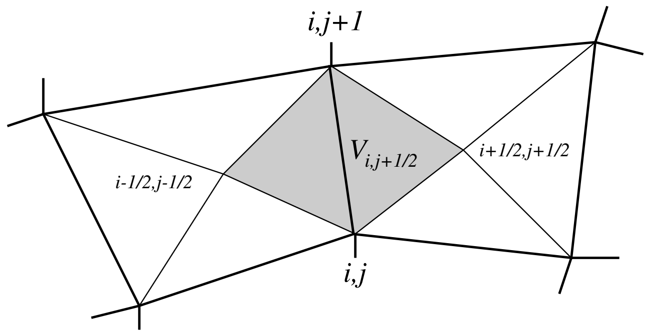

Fig. 8: The quadrilateral volume $V_{i,j+1/2}$ associated with edge $(i, j + 1/2)$ is shown as the shaded area. The thicker lines are the zone edges.

where all terms containing $\mathbf{T}_{\eta_{i+\frac{1}{2},j}}^{i+\frac{1}{2},j+\frac{1}{2}}$ have been collected.

We now have two expressions for $(\mathbf{G}, \mathbf{T})$ in a zone. Equating the expressions allows the two $\mathbf{G}_\xi$ and $\mathbf{G}_\eta$ vectors in a zone to be found by solving two independent local 4×4 sets of simultaneous equations, one for the x components and the second set for the y components. The main 4×4 matrix is the same for both components and is symmetric positive definite if the grid is not degenerate.

This derivation only allows us to find $\mathbf{G}_\xi$ and $\mathbf{G}_\eta$. This does not give us enough information to find $\mathbf{D}_\xi$ and $\mathbf{D}_\eta$. So this expression can only be used for the nonsymmetric form of the tensor viscosity.

6 Discrete form of tensor viscosity

In section 5 two separate sets of discrete equations were derived. In this section the implementation of the general form of the viscosity for each of the two sets is described.

6.1 Implementation for edge tangential projections

For the nonsymmetric viscosity, $\mathbf{G}$ is easily calculated. For the symmetric form it is not possible to then calculate $\mathbf{D}^\xi$ only from $\mathbf{G}^\xi$, and $\mathbf{D}^\eta$ only from $\mathbf{G}^\eta$. So we introduce a volume containing the edge, for which tensor $\mathbf{D}$ is calculated. The volume used is a quadrilateral whose four corners are the two nodes at either end of the edge and the centers of the two zones adjacent to the edge, this volume is shown in Fig. 8. The position and velocity of the zone centers are found by taking the average of the four surrounding nodes. $\mathbf{D}$ can then be calculated as

$$\mathbf{D}^\xi = \mathbf{G}^\xi - \mathbf{W}^\xi \quad , \quad \mathbf{D}^\eta = \mathbf{G}^\eta - \mathbf{W}^\eta. \tag{6.1}$$

The $\mathbf{G}^\xi$ and $\mathbf{G}^\eta$ terms are calculated using equation (5.4). Tensor $\mathbf{W}$ is the spin tensor and $\mathbf{W}^\xi$ and $\mathbf{W}^\eta$ are calculated using

$$\begin{aligned} \mathbf{W}^{\xi x} &= -\tfrac{1}{2}(\mathbf{curl}_k\ \mathbf{v}) \cdot \hat{\mathbf{e}}_{\xi x} \quad , \quad \mathbf{W}^{\xi y} = \tfrac{1}{2}(\mathbf{curl}_k\ \mathbf{v}) \cdot \hat{\mathbf{e}}_{\xi y} \\ \mathbf{W}^{\eta x} &= -\tfrac{1}{2}(\mathbf{curl}_k\ \mathbf{v}) \cdot \hat{\mathbf{e}}_{\eta x} \quad , \quad \mathbf{W}^{\eta y} = \tfrac{1}{2}(\mathbf{curl}_k\ \mathbf{v}) \cdot \hat{\mathbf{e}}_{\eta y} \end{aligned} \tag{6.2}$$

the form of $(\mathbf{curl}_k\ \mathbf{v})$ used is the usual finite difference expression, calculated for the quadrilateral volume associated with each edge.

For edge k, μ is defined as

$$\mu = (1-\psi_k)\rho_k \left\{ c_2 \frac{(\gamma-1)}{4}|\Delta\mathbf{v}_k| + \sqrt{c_2^2 \left(\frac{\gamma-1}{4}\right)^2 (\Delta\mathbf{v}_k)^2 + c_1^2 c_{s,k}^2} \right\} l_k. \tag{6.3}$$

The density, ρ_k, is calculated from the quadrilateral edge volume

$$\rho_k = \rho_k^0 \frac{V_k^0}{V_k} \tag{6.4}$$

where the superscript 0 denotes the initial values. This assumes that the volume associated with the edge is Lagrangian. $c_{s,k}$ is the average of the speed of sound in the two adjoining zones.

In order to keep the dimensions of the viscosity correct a characteristic length l_k has been added. For an edge the simplest definition of the length and the velocity jump, $\Delta\mathbf{v}$, would be to take the edge length and change in velocity over the edge. However with the tangential projection form of the discrete equations this choice did not give a robust viscosity. This version of the viscosity is most reliable when μ is not sensitive to direction, choosing the edge length and change in velocity gave μ too much directionality. So it was necessary to use a more complex definition.

The length is calculated by taking the square root of the edge volume and multiplying it by the square root of the aspect ratio. This gives a length that reflects the aspect ratio of the volume while being relatively insensitive to small changes in the velocity direction. The aspect ratio used is controlled by which of the two diagonals is closest in direction to the average velocity.

$$l_k = \begin{cases} \sqrt{V}\sqrt{\frac{|\Delta\mathbf{x}_k|}{|\Delta\mathbf{x}_{centers}|}} & \text{if} \quad \widehat{\Delta\mathbf{x}}_k \cdot \hat{\mathbf{v}}_{av} \leq \widehat{\Delta\mathbf{x}}_{centers} \cdot \hat{\mathbf{v}}_{av} \\ \sqrt{V}\sqrt{\frac{|\Delta\mathbf{x}_{centers}|}{|\Delta\mathbf{x}_k|}} & \text{if} \quad \widehat{\Delta\mathbf{x}}_k \cdot \hat{\mathbf{v}}_{av} > \widehat{\Delta\mathbf{x}}_{centers} \cdot \hat{\mathbf{v}}_{av}. \end{cases} \tag{6.5}$$

Fig. 9 shows how $\Delta\mathbf{x}_k$, $\Delta\mathbf{x}_{centers}$ and $\mathbf{v}_{av}$ are defined.

The change in velocity was taken to be the maximum velocity jump of the two diagonals

$$\Delta\mathbf{v} = \max(|\Delta\mathbf{v}_k|, |\Delta\mathbf{v}_{centers}|). \tag{6.6}$$

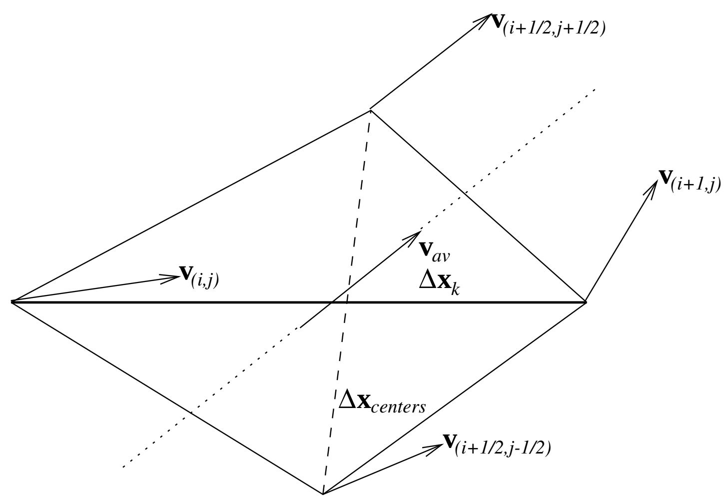

Fig. 9: The diagonal lengths $\Delta\mathbf{x}_k$ along the edge and $\Delta\mathbf{x}_{centers}$ and the average velocity $\mathbf{v}_{av}$ are used to calculate the length for the viscosity.

These definitions of length and velocity were chosen as in tests they results in a more robust code than the other definitions tried. Neither of these definitions rely on a good estimate of the shock direction. They are not too sensitive to direction, while allowing for low and high aspect ration zones.

Initially the same limiter as the edge viscosity was used. In tests of the viscosity it was observed that for problems where only shock compression occurs, results were improved by removing the limiter. A second limiter function was then developed that checks along both local coordinate axes.

$$\psi_k = \min(\psi_1, \psi_2) \tag{6.7}$$

where

$$\begin{aligned} \psi_1 &= \max[0, \min(0.5(r_{l,k} + r_{r,k}) \, , \, 2r_{l,k} \, , \, 2r_{r,k} \, , \, 1)] \\ \psi_2 &= \max[0, \min(0.5(r_{m,k} + r_{p,k}) \, , \, 2r_{m,k} \, , \, 2r_{p,k} \, , \, 1)]. \end{aligned} \tag{6.8}$$

If edge k is edge $(i+1/2, j)$ then

$$\begin{aligned} r_{l,k} &= \frac{(\mathbf{div}_k \ \mathbf{v})_{i-\frac{1}{2},j}}{(\mathbf{div}_k \ \mathbf{v})_{i+\frac{1}{2},j}} \quad , \quad r_{r,k} = \frac{(\mathbf{div}_k \ \mathbf{v})_{i+\frac{3}{2},j}}{(\mathbf{div}_k \ \mathbf{v})_{i+\frac{1}{2},j}} \\ r_{m,k} &= \frac{(\mathbf{div}_k \ \mathbf{v})_{i+\frac{1}{2},j-1}}{(\mathbf{div}_k \ \mathbf{v})_{i+\frac{1}{2},j}} \quad , \quad r_{p,k} = \frac{(\mathbf{div}_k \ \mathbf{v})_{i+\frac{1}{2},j+1}}{(\mathbf{div}_k \ \mathbf{v})_{i+\frac{1}{2},j}} \end{aligned} \tag{6.9}$$

$\mathbf{div}_k\ \mathbf{v}$ is calculated for the edge volume in the usual finite difference fashion. This form of ψ_k reduces to the same expression as the edge limiter in one dimension. Unlike the edge viscosity limiter, this limiter is not one on edges that are perpendicular to a uniform shock, but wave front invariance already is ensured by the viscosity formulation.

The edge viscosity was found to be insensitive to the type of boundary condition used when calculating ψ [6]. So r_l and r_r were set to 1.0 whenever they lie outside the boundary. It was found that the tensor viscosity was sensitive to the type of boundary condition used. So for a symmetry boundary condition r_r and r_l are calculated using the values known from the boundary condition. For a free surface they are still set to 1.0.

The final property required for μ is to be zero for expansion. For this the divergence for velocity is calculated for the edge volume, and μ is set to zero if this is positive, so

$$\mu = 0 \quad \text{if} \quad (\mathbf{div}_k\ \mathbf{v}) > 0. \tag{6.10}$$

For this version of the viscosity, equation (5.10) is used in the momentum equation to calculate the divergence of $\mathbf{Q}$. For the energy equation it is possible to use equation (5.7) to calculate the tensor scalar product in a zone. However the standard compatible hydrodynamics form of the energy equation is equivalent if the zone contributions to the total nodal force are known, referred to as a corner forces. The corner forces can be found from equation (5.10) by only considering terms which contain V and θ from a single zone. As the two equations are equivalent, dissipativity is still satisfied. Using the standard compatible hydrodynamics form of the energy equation is computationally cheaper than using equation (5.7).

6.2 Implementation for median normal projections

The objective with this version was to implement the tensor viscosity in a manner closer to the original edge viscosity than was possible with the edge tangential projection formulation. Using normal projections to the median mesh allows the viscosity to be calculated in the same triangular subzone volume, but unlike the edge viscosity all four nodes of the zone are considered when calculating the velocity gradient.

The nodal forces and velocity gradient are calculated using the equations from section 5.3. The zone internal energy is calculated using equation (5.15) which is the same as the expression used for the edge viscosity. Using the symmetric positive definite property of the 4×4 matrix it can be shown that using equation (5.15) ensures dissipativity.

In a subzone volume μ is defined as

$$\mu = (1 - \psi_k)\rho_k \left\{ c_2 \frac{(\gamma - 1)}{4} |\Delta \mathbf{v}_k| + \sqrt{c_2^2 \left(\frac{\gamma - 1}{4} \right)^2 (\Delta \mathbf{v}_k)^2 + c_1^2 c_{s,k}^2} \right\} l_k \tag{6.11}$$

where ρ is calculated assuming the triangular volume is Lagrangian. $c_{s,k}$ is the same as used for the edge viscosity. The length and velocity are taken from the edge, so l_k is the edge length and $\Delta\mathbf{v}$ is the velocity difference between the two nodes at either end of the edge.

The limiter function ψ_k is the same as used for the edge viscosity. This viscosity was also found to be sensitive to the boundary conditions used when calculating ψ. For a symmetry boundary condition r_r and r_l are calculated using the values known from the boundary condition. For a free surface they are set to 1.0.

7 Test results

The tensor artificial viscosity was implemented in a test code. The test code is a Lagrangian finite difference code which uses a compatible hydrodynamics algorithm [15]. The test code uses the Lagrangian subzonal pressure method to control grid distortion [16], and contains the edge viscosity developed by Caramana et al. [6] which is briefly described in section 2. Therefore we have one code which contains both the edge viscosity and the tensor viscosity, so when comparing results the only difference in the code used to produce them is the viscosity routines.

As the viscosity has only been described in two dimensions, we only present test problems in two dimensional plane geometry. To avoid interaction of the subzonal pressures and the artificial viscosity obscuring differences in the viscosities, where possible the subzonal pressures method was switched off (merit factor = 0.0). Where subzonal pressures are required to allow the problem to run to the set time, the merit factor used is given.

Four principal test problems were used to investigate the behavior of the tensor viscosities. For all problems and viscosities the coefficients c_1 and c_2 were both set to 1.0. With the tensor tangential viscosity, the new limiter function is used as the default.

7.1 Noh implosion problem

The Noh problem [7] is a well known test problem. Here the cylindrical implosion problem is used. A perfect gas with $\gamma = 5/3$ is given an initial unit inward radial velocity. A circular shock wave is generated at the center of convergence. At time 0.6 this shock wave has a radial coordinate of 0.2. The initial and final conditions for this problem are given in table 1. Ahead of the shock the gas is compressed due to the convergence, and this produces a density profile with the equation $\rho = 1 + (t/R)$ where R is the radial coordinate and t the time.

Results are shown for both Cartesian and polar meshes. The Cartesian mesh is 50×50 zones, with the length of each edge is 1.0. The polar mesh has an initial radius of 1.0, with 50 zones radially. The angular zoning varies, and is specified for each set of results. Only a quarter of the volume is modeled, symmetry boundary conditions are used along the x and y axes.

	Initial	Final
Density	1.0	16.0
Pressure	0.0	16/3
Internal Energy	0.0	0.5
Shock Velocity	1/3	-

Table 1: Initial and final conditions for cylindrical Noh implosion problem.

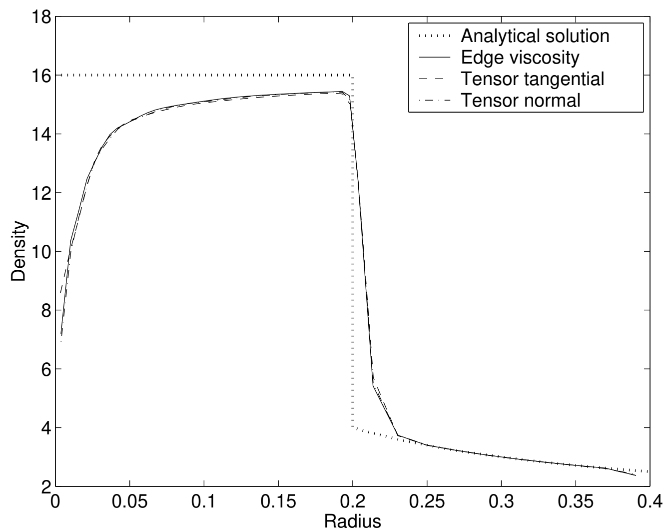

Fig. 10: Noh problem results on a polar mesh, with 3° angular zoning, for all three viscosities.

On a polar mesh all viscosities give very similar results, Fig. 10 shows density profiles for all viscosities for a mesh with fine, 3°, angular zoning. Results from a mesh with coarse, 45°, angular zoning show only minor variations in the density profiles.

The Noh problem for a Cartesian mesh is a test problem where the edge viscosity fails, Fig. 11. Along the axes jets form which result in a highly distorted mesh, subzonal pressures are required to allow the calculation to reach time 0.6. Increasing the merit factor just results in the jets becoming even more pronounced. The mesh can be improved by the c_1 viscosity coefficient to around 3.75 or higher, but this gives an error in the shock location and a very uneven density behind the shock, Fig. 12.

The tensor tangential and tensor normal viscosities both produce a smooth mesh behind a circular shock, Figs. 13, 14. The symmetric and nonsymmetric tensor tangential viscosities both give very similar results, so only the nonsymmetric are shown. Comparing the Cartesian mesh results with the polar shows

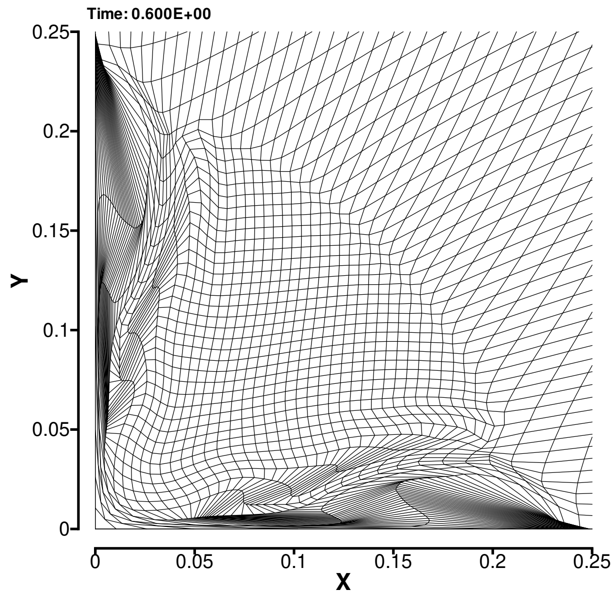

a

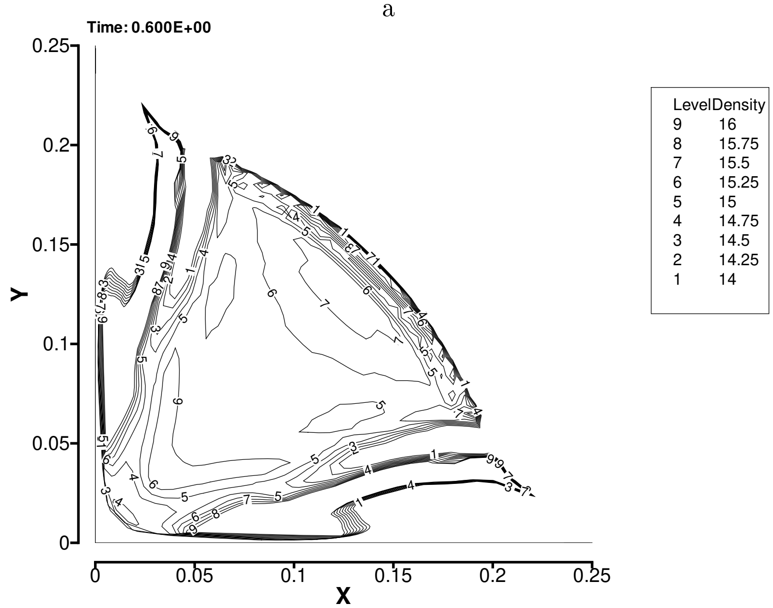

b

Fig. 11: Noh problem results on a Cartesian mesh for edge viscosity, merit factor = 0.05. (a) Mesh. (b) Density contour plot.

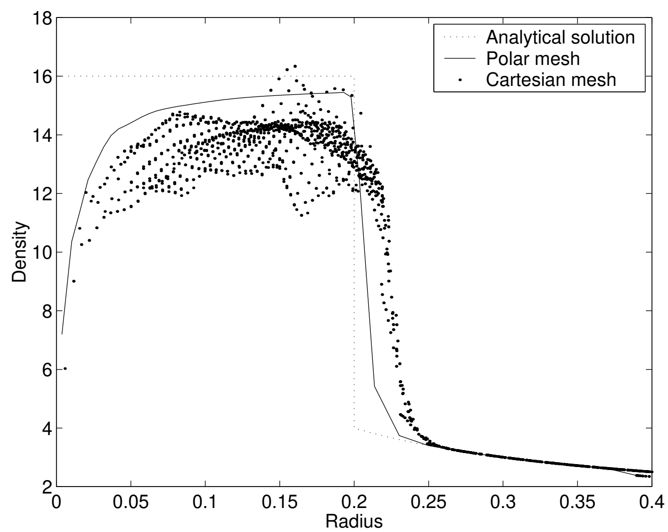

Fig. 12: Comparison of Noh problem results for polar ($c_1 = 1.0$) and Cartesian ($c_1 = 3.75$) meshes for edge viscosity. For the Cartesian mesh each point is a zone density plotted for the radius of the zone center.

good agreement in shock location and density behind the shock for both viscosities, Figs. 15, 16. The tensor normal viscosity gives less variation in density for a given radius than the tensor tangential viscosity, but does have some oscillation behind the shock around the $x = y$ line.

7.2 Saltzman Piston

In the Saltzman piston problem [8] a one dimensional shock wave propagates through a two dimensional mesh. This tests the ability of the code to model shock waves that are oblique to the mesh. As artificial viscosity is dominant in shock wave propagation, the Saltzman piston problem has often been used as in testing artificial viscosities [5, 8, 17].

The problem takes a box filled with gas, one end of the box is a movable piston. The piston moves into the box with a constant velocity of 1.0 and a strong shock wave is generated from the moving end. The gas is modelled using the ideal gas equation of state with $\gamma = 5/3$. Table 2 gives the initial conditions and exact results for the problem, the first shock is generated by the motion of the piston, the second shock is the reflection of the first shock off the fixed end, the third shock is the reflection of the second off the moving end.

The initial mesh is shown in Fig. 17. The initial length (x) is 1.0, and the height (y) is 0.1. The mesh is 100 zones in the x direction and 10 in the y direction. On the upper and lower boundaries symmetry boundary conditions are used. The nodal x coordinates are given as a function of their logical coordinates

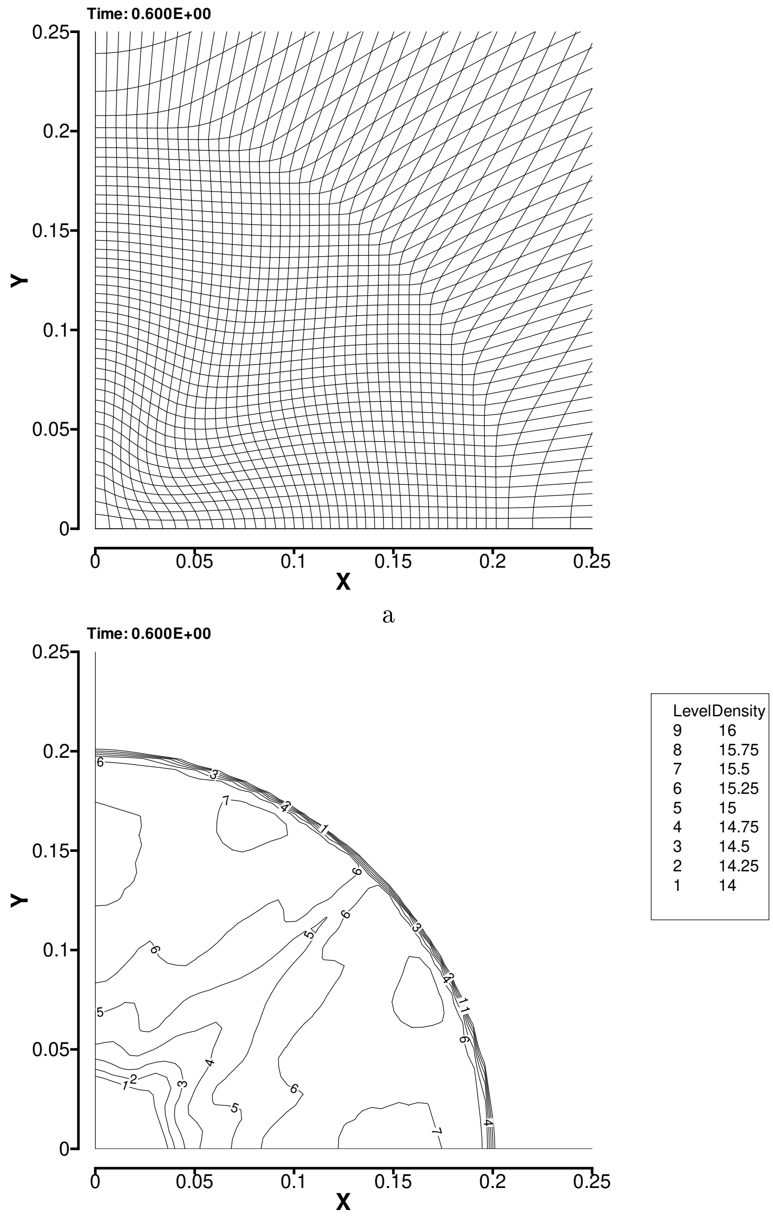

Fig. 13: Noh problem results on a Cartesian mesh for nonsymmetric tensor tangential viscosity, merit factor = 0.0. (a) Mesh. (b) Density contour plot.

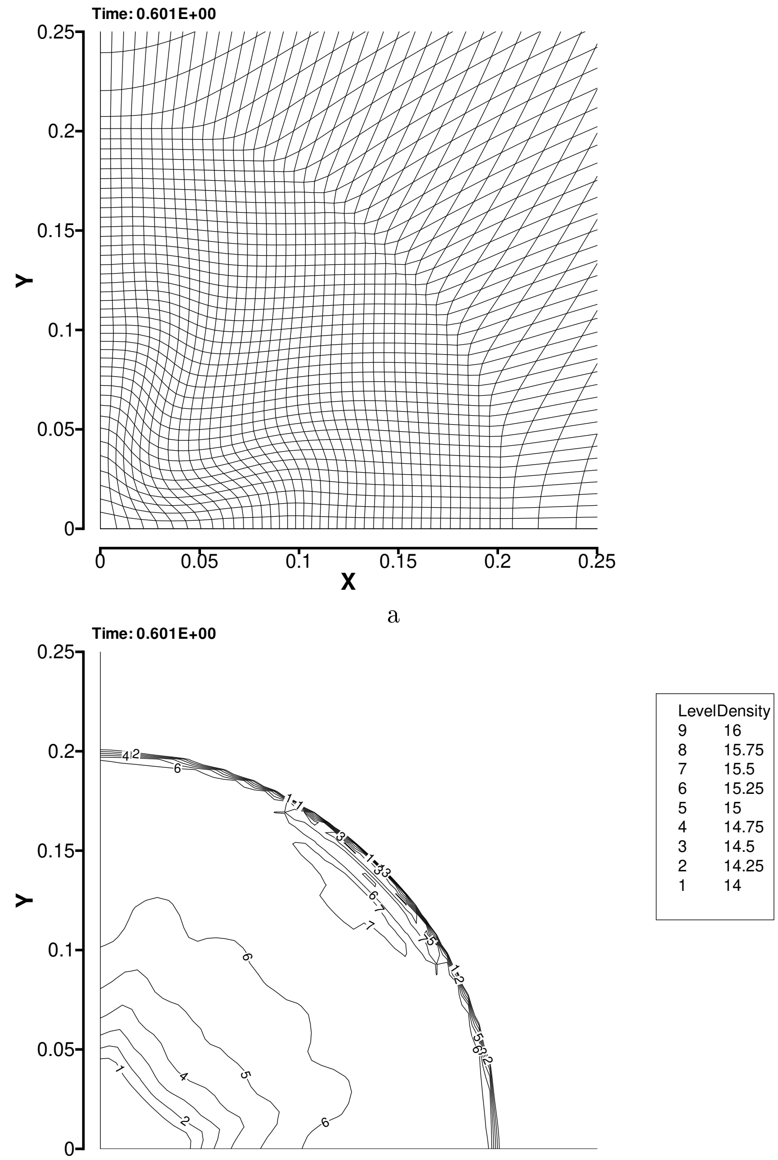

Fig. 14: Noh problem results on a Cartesian mesh for tensor normal viscosity, merit factor = 0.0. (a) Mesh. (b) Density contour plot.

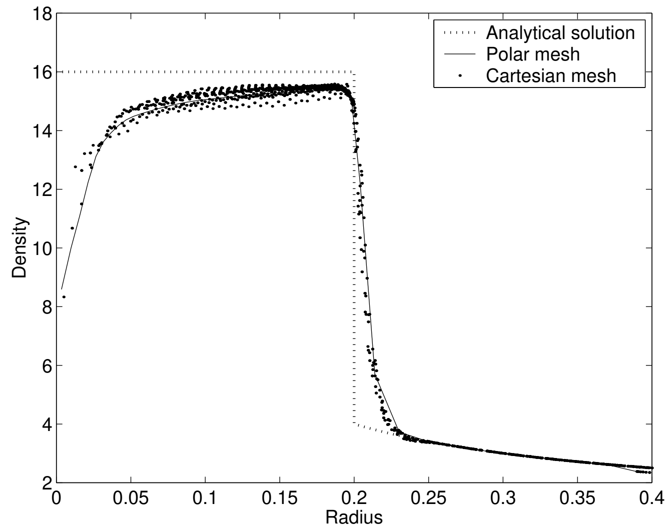

Fig. 15: Comparison of Noh problem results for polar and Cartesian meshes for nonsymmetric tensor tangential viscosity. For the Cartesian mesh each point is a zone density plotted for the radius of the zone center.

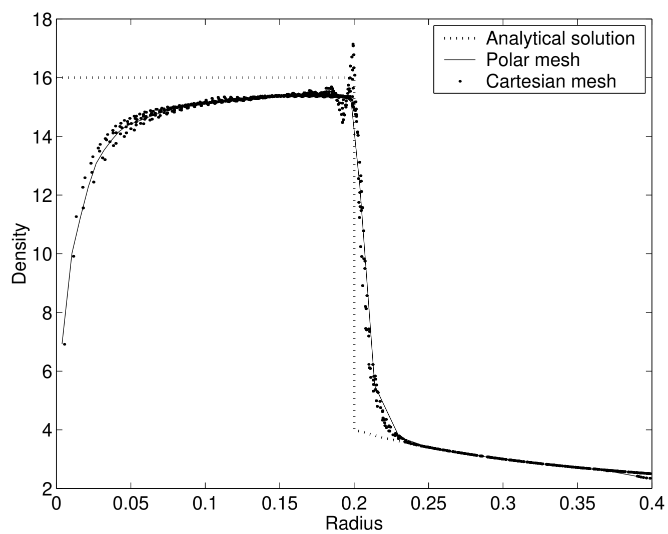

Fig. 16: Comparison of Noh problem results for polar and Cartesian meshes for tensor normal viscosity. For the Cartesian mesh each point is a zone density plotted for the radius of the zone center.

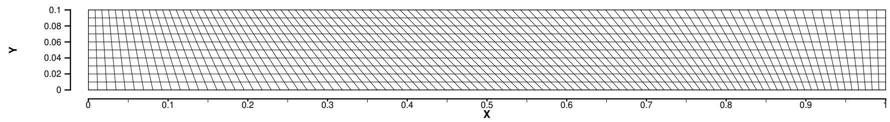

Fig. 17: Initial mesh for Saltzman piston problem. The piston moves from left to right at constant velocity.

i, j by

$$x(i,j) = (i-1)dx + (11-j)\sin\left(\frac{\pi(i-1)}{100}\right)dy \tag{7.1}$$

where $dx = 1/100$ and $dy = 0.1/10$.

Two additional variants of this problem were also used, both change only the maximum y coordinate. The shock velocity and final conditions are unchanged. In practical problems it is often not possible to keep zone aspect rations close to 1:1. The first variant changes the maximum y coordinate to 0.05. This gives zones with an initial aspect ratio of 2:1, and which are longer in the direction normal to the shock wave. As the critical time step is controlled by the smallest zone direction, long thin zones can cause the viscosity to exert force on nodes before the shock should have physically reached them. In the second variant the maximum y coordinate is 10, giving an aspect ratio of 1:100. This variant was first used by Margolin [8] to test his viscosity.

Results are shown at time 0.7 for all variants, and at time 0.925 for the 1:1 variant only. At time 0.7 the shock has an x coordinate of 0.9333, and has not yet reached the fixed end. By time 0.925, the shock has an x coordinate of 0.95, and is the third shock having reflected off the fixed and then moving ends.

All viscosities give good results for the 1:1 Saltzman piston problem at time 0.7, Figs. 18–21. With the tensor tangential viscosity giving the smallest density error at the boundaries.

To reach time 0.925 using the edge viscosity subzonal pressures are required,

	Initial	First shock	Second shock	Third shock
Density	1.0	4.0	10	20
Pressure	0.0	4/3	8	28
Internal Energy	1.0×10^{-4}	0.5	1.2	2.1
Shock Velocity	-	4/3	2/3	2
Final time	-	0.8	0.9	0.95

Table 2: Exact results for Saltzman piston problem. The density, pressure and internal energy are the values behind the shock. The shock velocity is with respect to the fixed coordinate system. The final time gives the time that the shock wave reaches an end of the box

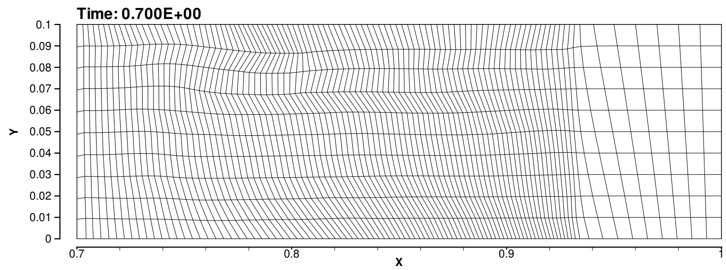

a

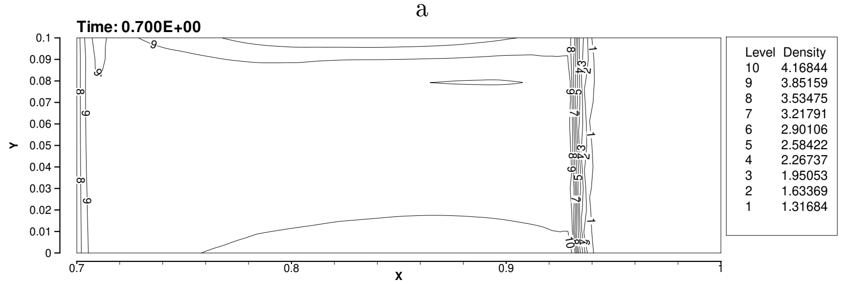

b

Fig. 18: 1:1 Saltzman piston results for edge viscosity, merit factor = 0.0. (a) Mesh. (b) Density contour plot.

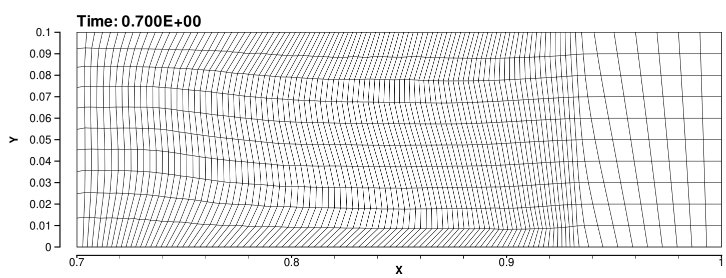

a

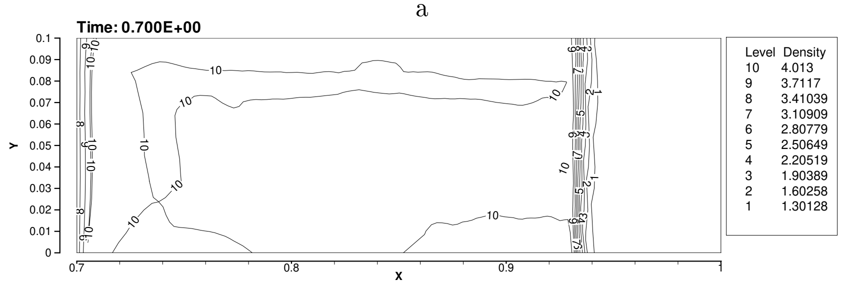

b

Fig. 19: 1:1 Saltzman piston results for symmetric tensor tangential viscosity, merit factor = 0.0. (a) Mesh. (b) Density contour plot.

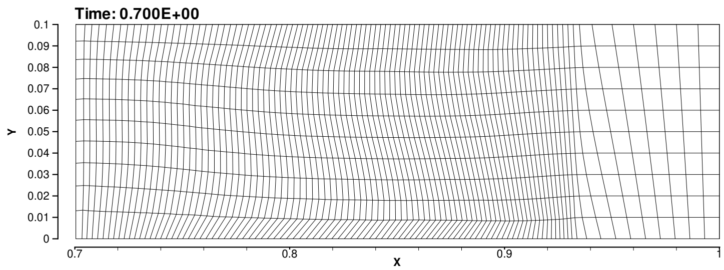

a

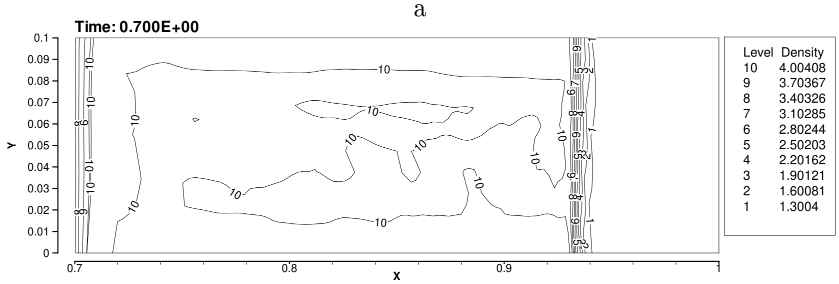

b

Fig. 20: 1:1 Saltzman piston results for nonsymmetric tensor tangential viscosity, merit factor = 0.0. (a) Mesh. (b) Density contour plot.

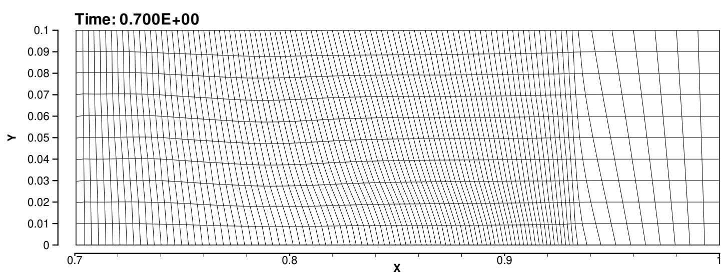

a

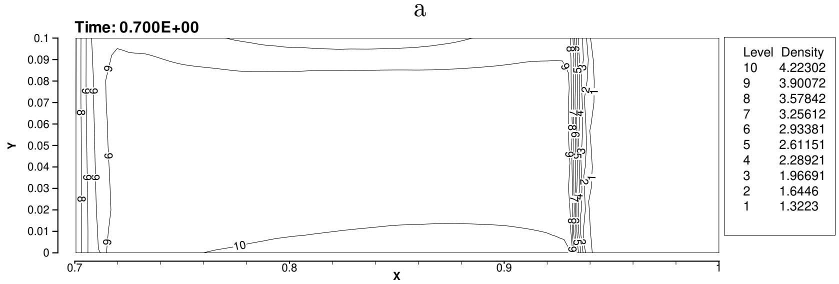

b

Fig. 21: 1:1 Saltzman piston results for tensor normal viscosity, merit factor = 0.0. (a) Mesh. (b) Density contour plot.

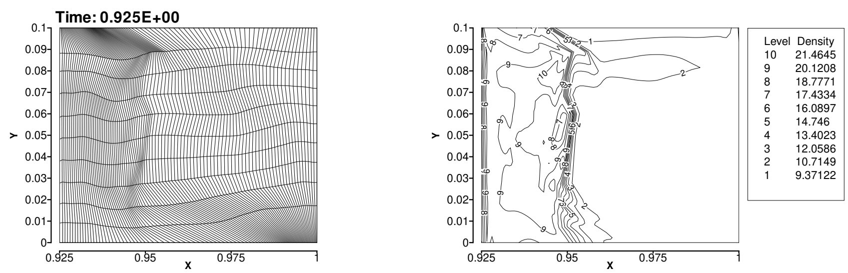

a b

Fig. 22: 1:1 Saltzman piston results for edge viscosity at t=0.925, merit factor = 0.1 (a) Mesh. (b) Density contour plot.

otherwise the calculation stops shortly before time 0.925 due to mesh problems. The results for a merit factor of 0.1 show that the shock wave is no longer planer near the boundaries, Fig. 22. Increasing the merit factor produces a more even final mesh. The tensor viscosity results all show a planar shock at time 0.925 with a merit factor of 0.1, Figs. 23–25.

For the 1:100 variant all viscosities give very similar results, Figs. 26–29. The shock waves are not planar near the boundaries, but increasing the subzonal pressure merit factor produces a more planar shock for all viscosities, this was shown for the edge viscosity in [16].

The 2:1 variant is where the Saltzman problem shows the clearest differences between the viscosities. The edge viscosity shows mesh distortion along the top and bottom boundaries, Fig. 30, in this case the addition of subzonal pressures makes the mesh distortion on the lower edge more pronounced. The symmetric tensor tangential viscosity using the edge viscosity limiter produces a very distorted mesh near the piston, Fig. 31. Using the new limiter it could not successfully reach time 0.7, even using subzonal pressures. The nonsymmetric tensor tangential viscosity gives similar results to the symmetric viscosity using the edge limiter, Fig. 32, but now using the new limiter gives good results, a planar shock and a smooth mesh, Fig. 33. The tensor normal viscosity also gives good results for this variant.

The most noticeable differences between the viscosities are seen at time 0.925 for the 1:1 variant, and for the 2:1 variant. The tensor tangential viscosity generally gives the smoothest density results. In his 1993 paper [17] Benson observes that for this problem it is generally true that a narrower shock results in a less uniform density behind the shock. All the three viscosities give a similar shock front width of approximately 3–4 zones, so the shock width is not causing the variation in the smoothness of the density field.

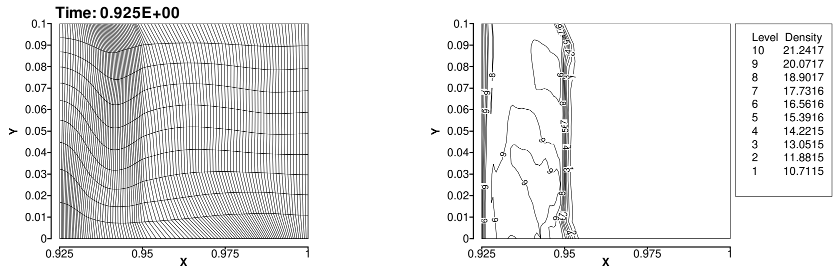

a b

Fig. 23: 1:1 Saltzman piston results for symmetric tensor tangential viscosity at t=0.925, merit factor = 0.1 (a) Mesh. (b) Density contour plot.

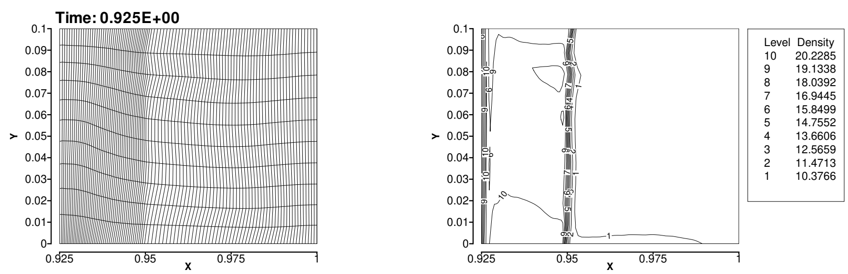

a b

Fig. 24: 1:1 Saltzman piston results for nonsymmetric tensor tangential viscosity at t=0.925, merit factor = 0.1 (a) Mesh. (b) Density contour plot.

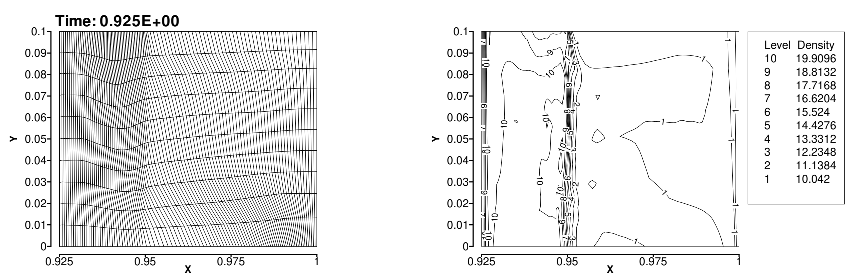

a b

Fig. 25: 1:1 Saltzman piston results for tensor normal viscosity at t=0.925, merit factor = 0.1 (a) Mesh. (b) Density contour plot.

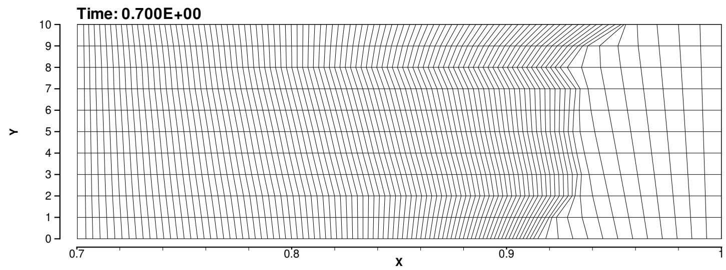

a

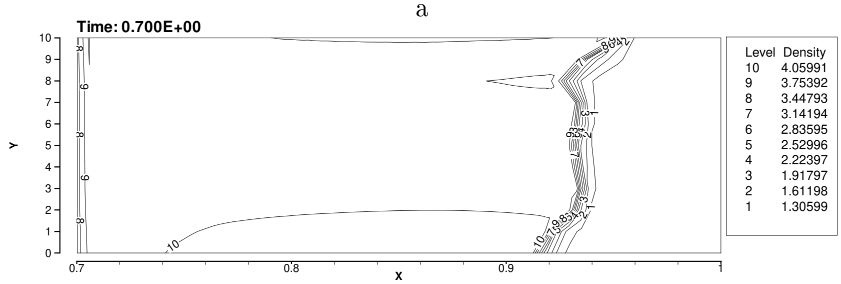

b

Fig. 26: 1:100 Saltzman piston results for edge viscosity. Merit factor = 2.0. (a) Mesh. (b) Density contour plot.

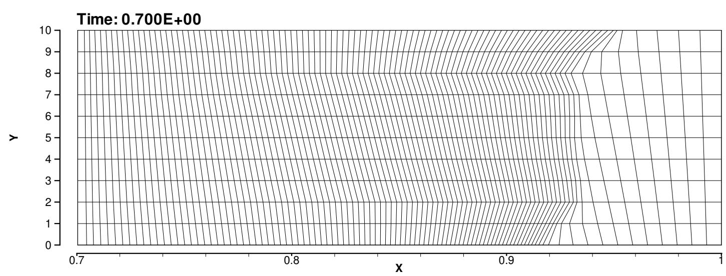

a

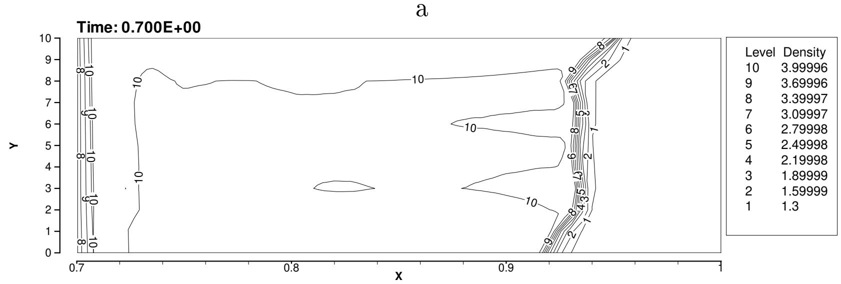

b

Fig. 27: 1:100 Saltzman piston results for symmetric tensor tangential viscosity, merit factor = 2.0. (a) Mesh. (b) Density contour plot.

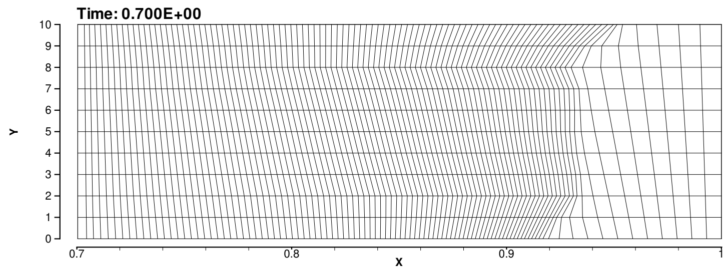

a

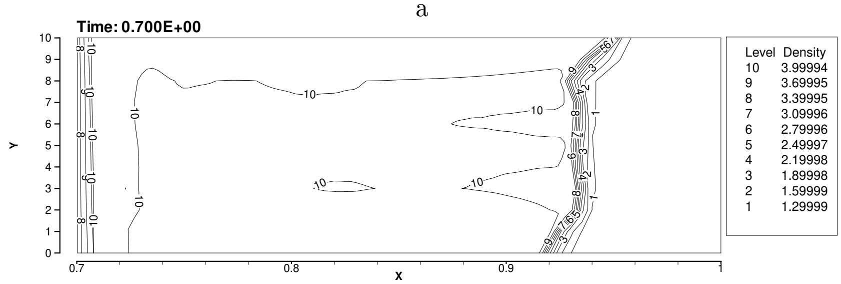

b

Fig. 28: 1:100 Saltzman piston results for nonsymmetric tensor tangential viscosity, merit factor = 2.0. (a) Mesh. (b) Density contour plot.

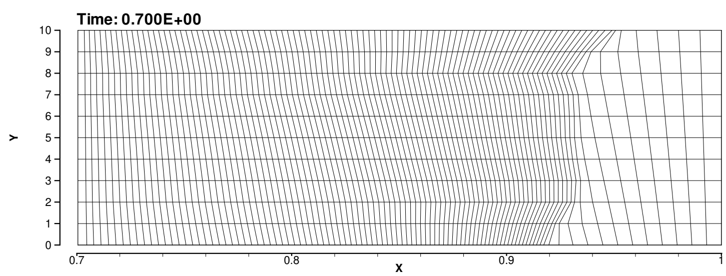

a

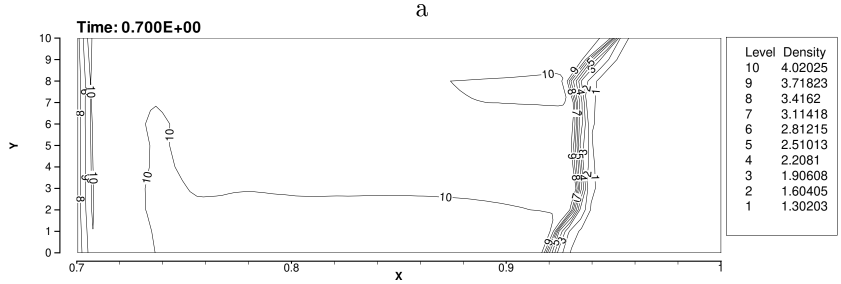

b

Fig. 29: 1:100 Saltzman piston results for tensor normal viscosity, merit factor = 2.0. (a) Mesh. (b) Density contour plot.

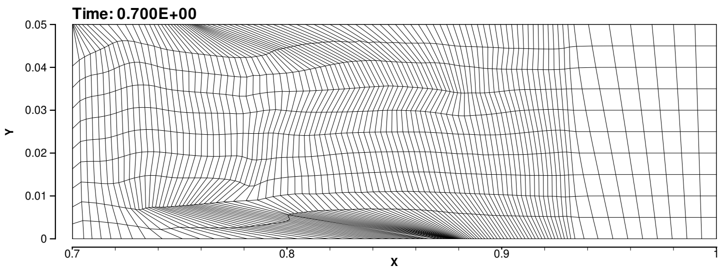

a

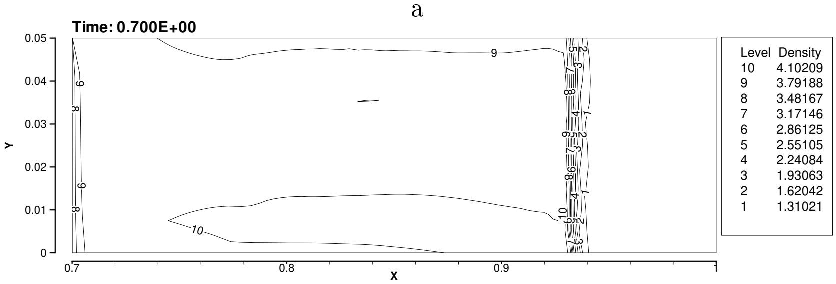

b

Fig. 30: 2:1 Saltzman piston results for edge viscosity, merit factor = 0.0.. (a) Mesh. (b) Density contour plot.

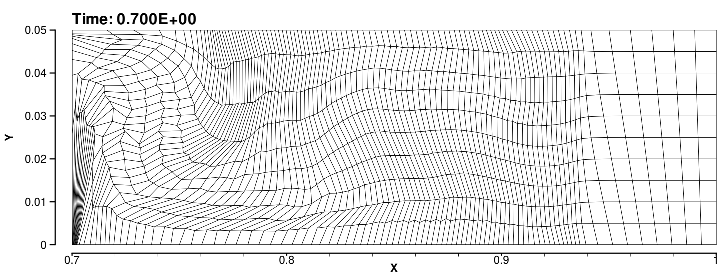

a

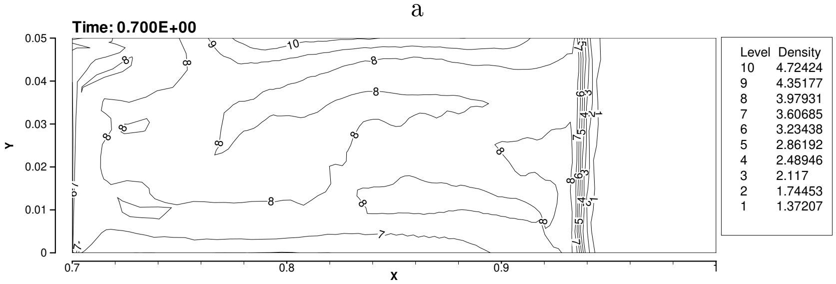

b

Fig. 31: 2:1 Saltzman piston results for symmetric tensor tangential viscosity, merit factor = 0.0. Edge viscosity limiter function. (a) Mesh. (b) Density.

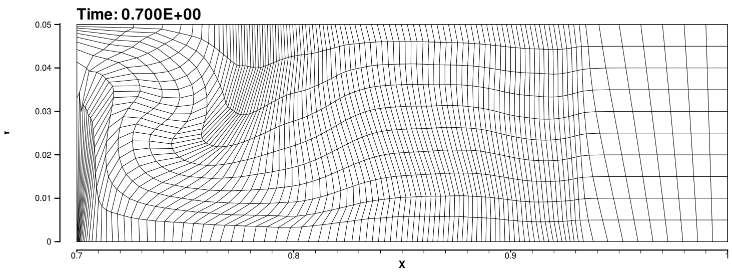

a

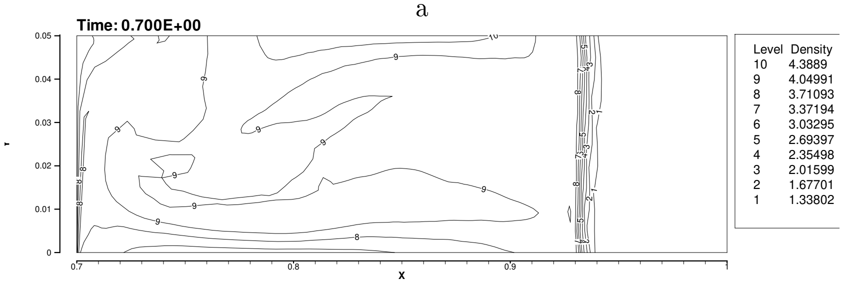

b

Fig. 32: 2:1 Saltzman piston results for nonsymmetric tensor tangential viscosity, merit factor = 0.0. Edge viscosity limiter function. (a) Mesh. (b) Density.

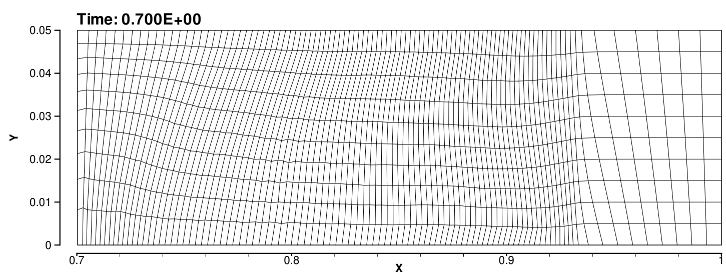

a

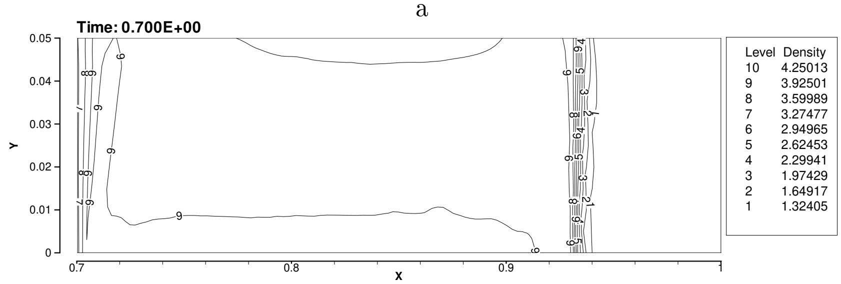

b

Fig. 33: 2:1 Saltzman piston results for nonsymmetric tensor tangential viscosity, merit factor = 0.0. New limiter function. (a) Mesh. (b) Density.

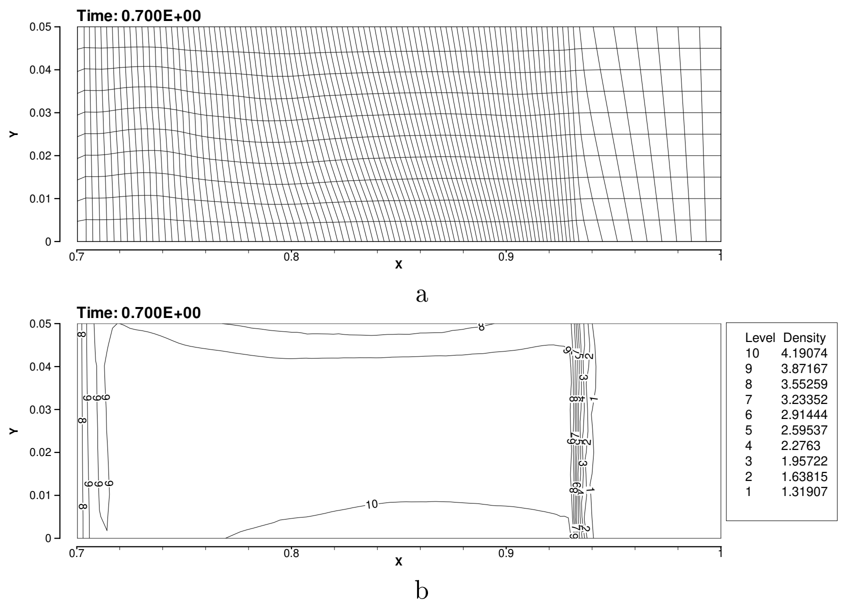

Fig. 34: 2:1 Saltzman piston results for tensor normal viscosity, merit factor = 0.0. (a) Mesh. (b) Density contour plot.

7.3 Sedov blast wave problem

The Sedov blast wave [18] problem models the blast wave from an intense explosion in a perfect gas, so is an example of a diverging shock wave. The initial mesh is Cartesian, consisting of 45×45 zones with a total edge length of 1.1. The initial internal energy is zero except for the first zone, which has a specific internal energy of 409.7. The analytic solution gives, for $\gamma = 1.4$, a shock of radius unity at time unity, and with a peak density of 6.0.

For this problem both the edge and tensor tangential viscosities give good results, Figs. 35,36. Again the symmetric and nonsymmetric tensor tangential viscosities give very similar results. The edge viscosity does have a distorted mesh near the axes, but this problem does not grow or cause problems. The tensor normal viscosity gives an uneven shock front and mesh, Fig. 37.

The Sedov problem was also calculated on a different mesh with initially rectangular zones. The initial mesh is 45×90 zones, again with an total side length of 1.1. Two zones are given a specific internal energy of 409.7, so the initial state is equivalent to the square mesh. This is a tougher test of the ability of the code to preserve symmetry.

For this mesh subzonal pressures have to be used for all viscosities for the calculation to reach time 1.0, for each calculation a merit factor of 0.375 was used. The edge viscosity now gives an elliptical shock front, with a larger radius along the x axis (45 zones) than the y axis (90 zones), Fig. 38. The tensor

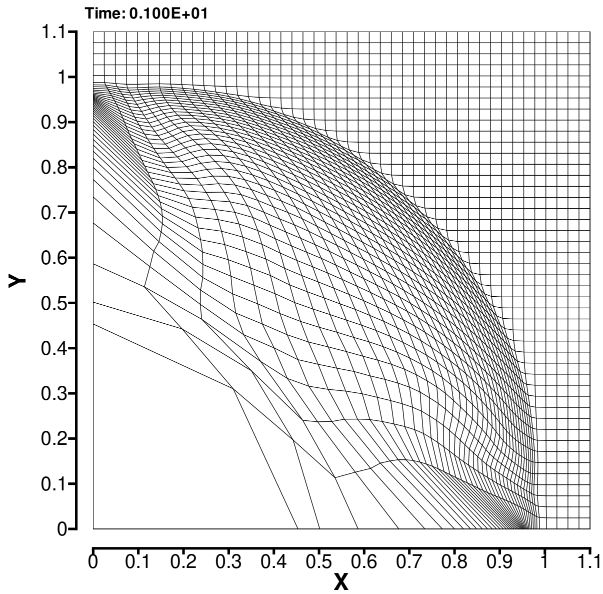

a

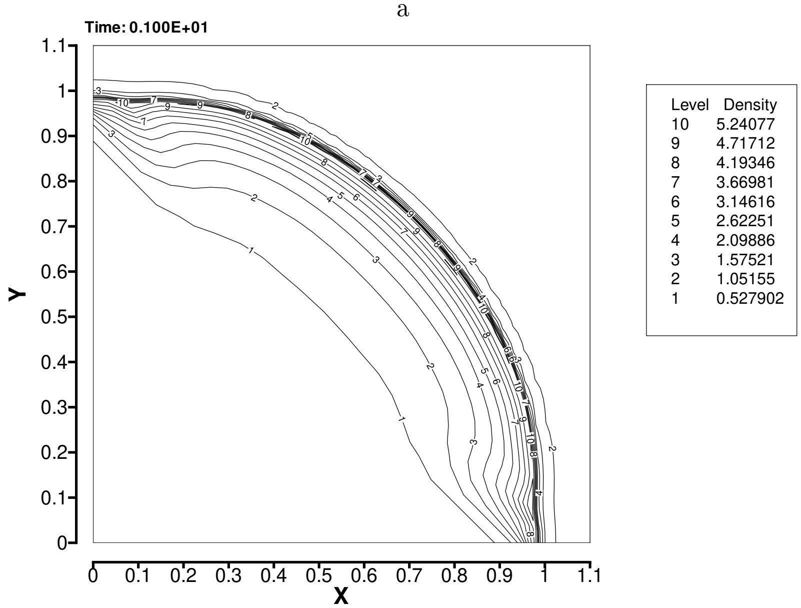

b

Fig. 35: Sedov problem results for edge viscosity, merit factor = 0.1. (a) Mesh. (b) Density contour plot.

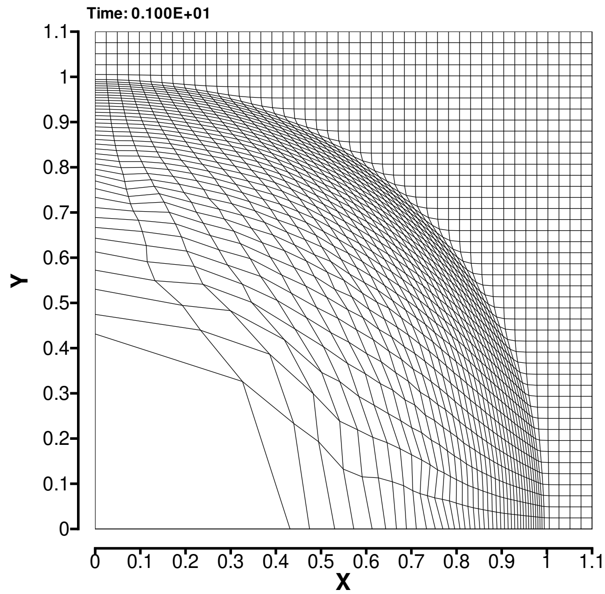

a

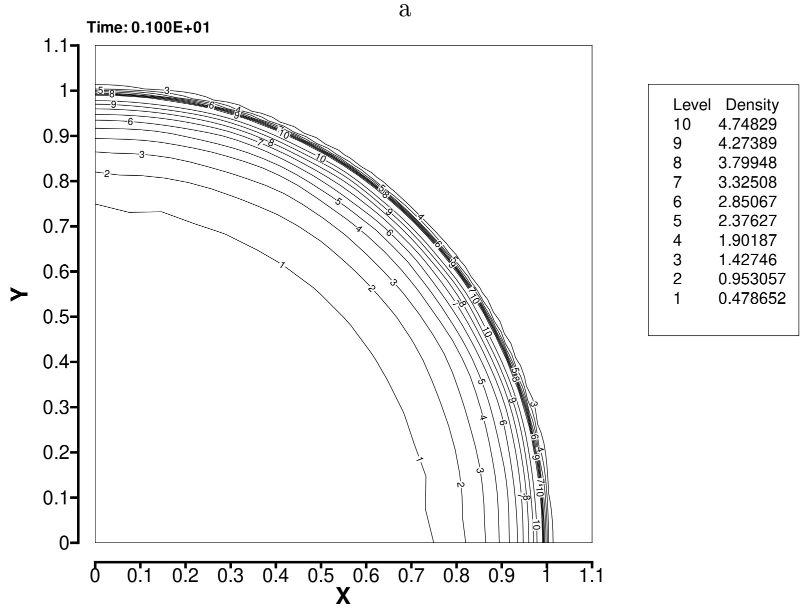

b

Fig. 36: Sedov problem results for nonsymmetric tensor tangential viscosity, merit factor = 0.1. (a) Mesh. (b) Density contour plot.

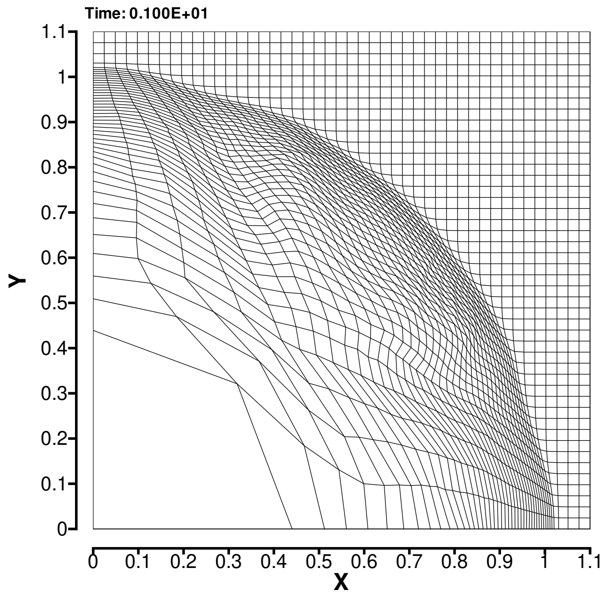

a

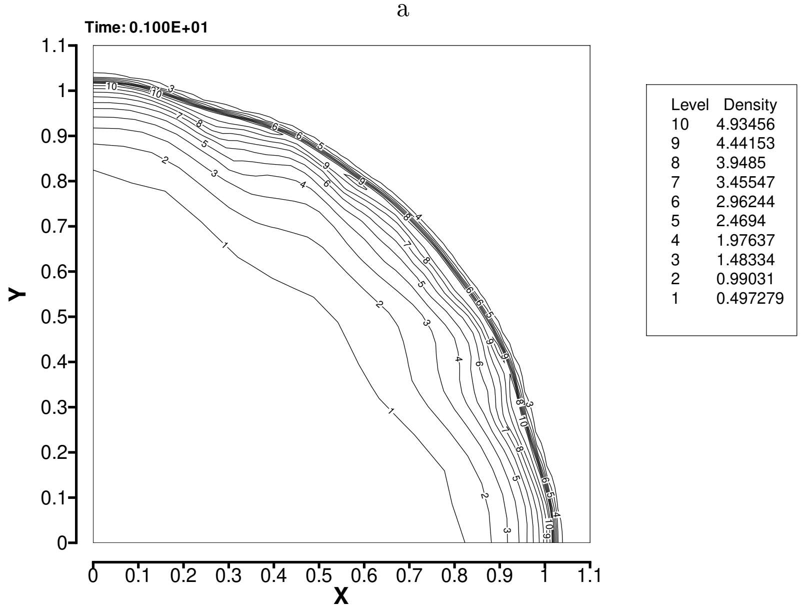

b

Fig. 37: Sedov problem results for tensor normal viscosity, merit factor = 0.1. (a) Mesh. (b) Density contour plot.

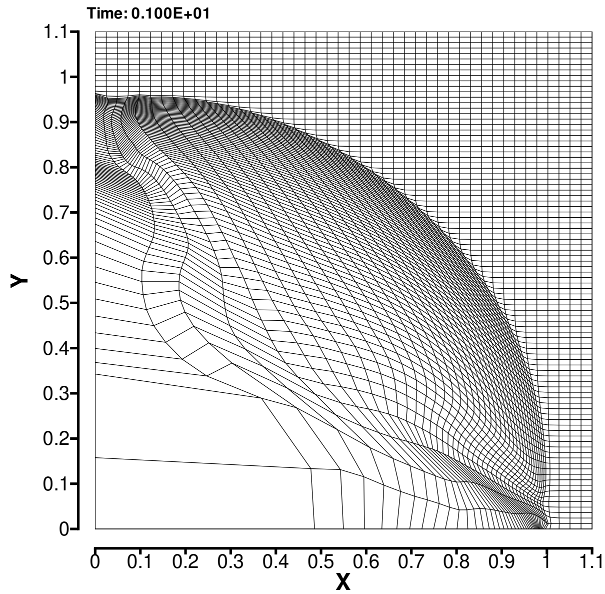

a

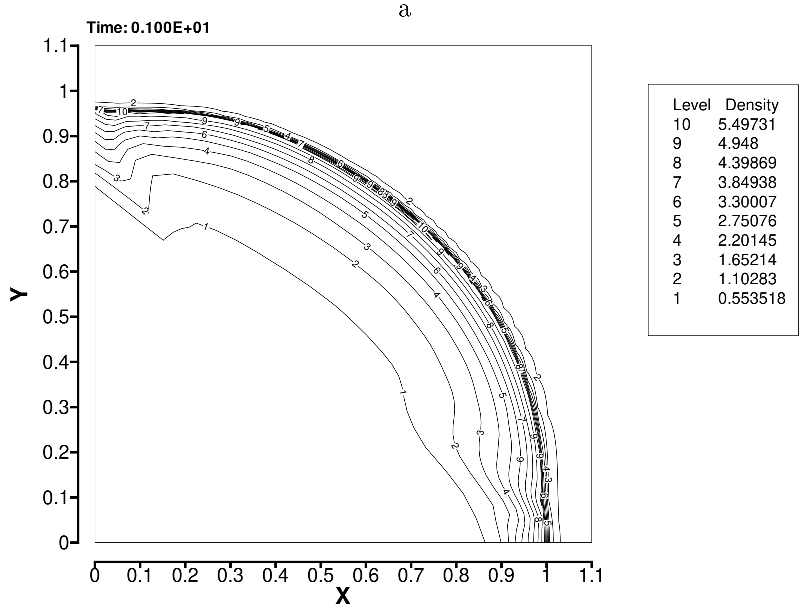

b

Fig. 38: 1:2 Sedov problem results for edge viscosity, merit factor = 0.375. (a) Mesh. (b) Density contour plot.

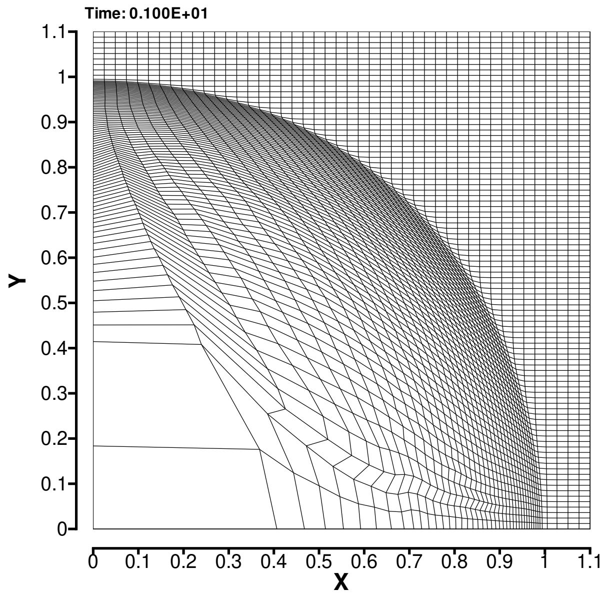

a

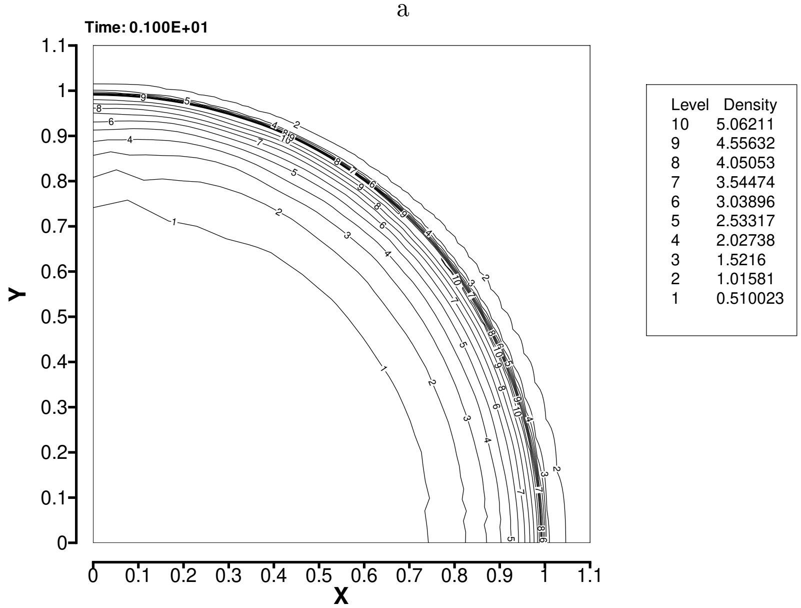

b

Fig. 39: 1:2 Sedov problem results for nonsymmetric tensor tangential viscosity, merit factor = 0.375. (a) Mesh. (b) Density contour plot.

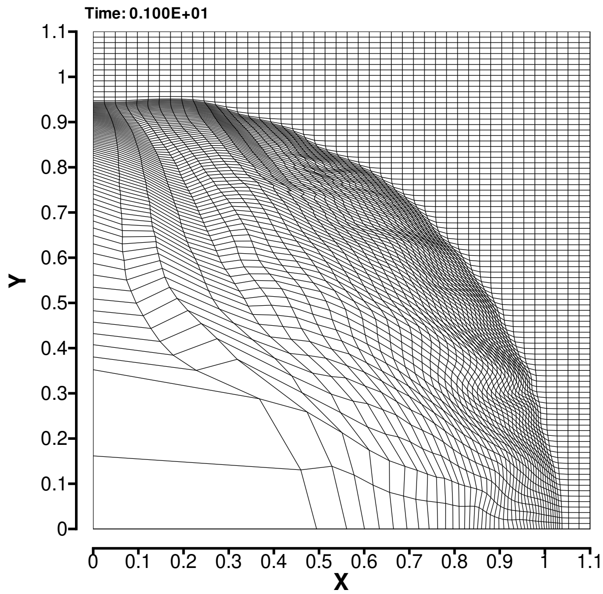

a

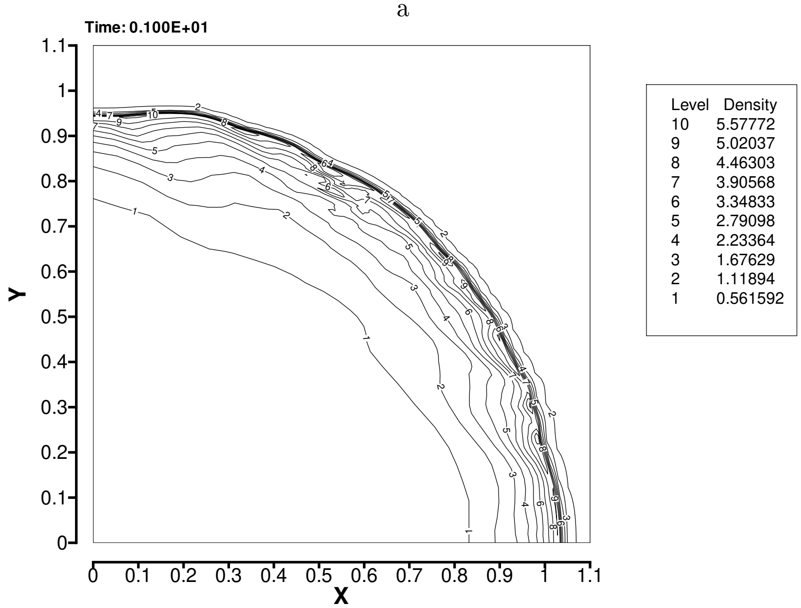

b

Fig. 40: 1:2 Sedov problem results for tensor normal viscosity, merit factor = 0.375. (a) Mesh. (b) Density contour plot.

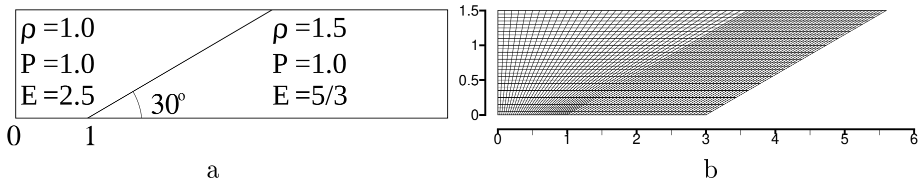

Fig. 41: Initial conditions (a), and initial mesh (b) for Dukowicz problem.

tangential viscosity gives a smooth mesh but unlike the edge viscosity retains a circular shock, Fig. 39. The tensor normal viscosity gives the worst result, with a clearly elliptical and uneven shock front, Fig. 40.

7.4 Dukowicz shock refraction problem

The Dukowicz problem is a two dimensional shock refraction problem on a mesh designed by Dukowicz and Meltz [19]. It is a useful problem as a vortex sheet is generated by the interaction of a shock with an inclined interface, and the mesh is uneven.

The problem takes two adjacent regions of gas with different densities, Fig. 41, with the interface between then aligned at 30° to the horizontal. In both regions $\gamma = 1.4$.

The mesh differs between the two regions. The fist region has 36×30 zones, with a vertical left boundary and a right boundary at 60° to the vertical. The second region is 40×30, with both left and right boundaries at 60° to the vertical.

A piston moves from the left with velocity 1.48, sending a shock ahead of it. The problem is run to a time of 1.3, just before the shock would leave the second region. The solution to the problem is shown in Fig. 42, as this assumes an infinite medium it is only correct until reached by the reflection from the bottom.

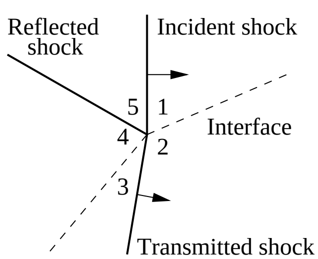

Region	1	2	3	4	5
Angle	60	131.02	21.90	90.96	56.12
Density	1	1.5	4.29	2.93	2.67
Pressure	1	1	5.15	5.15	4.50

Fig. 42: Exact results for Dukowicz problem, only valid away from the boundaries.

The edge viscosity requires subzonal pressures to prevent mesh tangling along the lower boundary, so all calculations used a merit factor of 0.1. Away from the boundaries the edge viscosity shows the expected shock wave pattern, Fig. 43. The interface along with the incident and transmitted shocks are clear, the reflected shock does not show clearly due to the small difference in density across it.

This is a problem where a clear difference can be seen between the symmetric and nonsymmetric forms of the tensor tangential viscosity, Figs. 44,45. The mesh quality of the nonsymmetric is clearly better, as the symmetric viscosity produces an uneven mesh. Both do show the expected shock structure.

For the tensor normal viscosity there is an overshoot in density immediately behind the shock in the second region that gives an oscillation behind the shock that is visible in the mesh, Fig. 46.

All the new viscosities produce a smoother mesh on the lower boundary than the edge viscosity. The smoothest overall mesh is for the nonsymmetric tensor tangential viscosity.

7.5 General discussion

The relative computational cost of each viscosity was checked by measuring the CPU time required for each artificial viscosity. The ratio between the edge viscosity cost and the cost of each new viscosity was measured for four problems: 1:1 Saltzman, Dukowicz, Sedov and Noh on a coarse polar mesh. Each problem was timed with and without compiler optimization. It was found that the ratio varied from problem to problem, with the Saltzman problem always giving the largest ratio. Table 3 summarizes these results. Approximately the tensor tangential viscosity is about 4 times as expensive as the edge viscosity with compiler optimization, while the tensor normal viscosity is about 2.5 times as expensive.

	Edge	Tensor Tangential	Tensor Normal
No compiler optimization (-O0)	1.0	4.0–5.3	3.1–4.1
With compiler optimization (-O4)	1.0	3.0–4.4	2.15–3.0

Table 3: Ratio of new viscosity CPU cost to edge viscosity cost, with and without compiler optimization.

Comparing the symmetric and nonsymmetric tensor tangential viscosities, where there is a difference between them the non-symmetric produces better results. When using the edge viscosity limiter again the nonsymmetric form produces better overall results. Of the two limiter functions tried for the tensor tangential viscosity, results using the new limiter function generally show an improved mesh over the edge limiter. In discussing the overall results, references to the tensor tangential viscosity will mean the nonsymmetric viscosity using the new limiter.

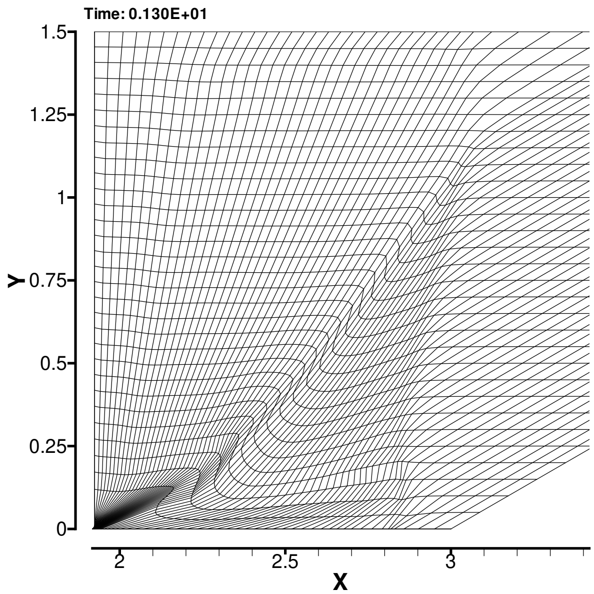

a

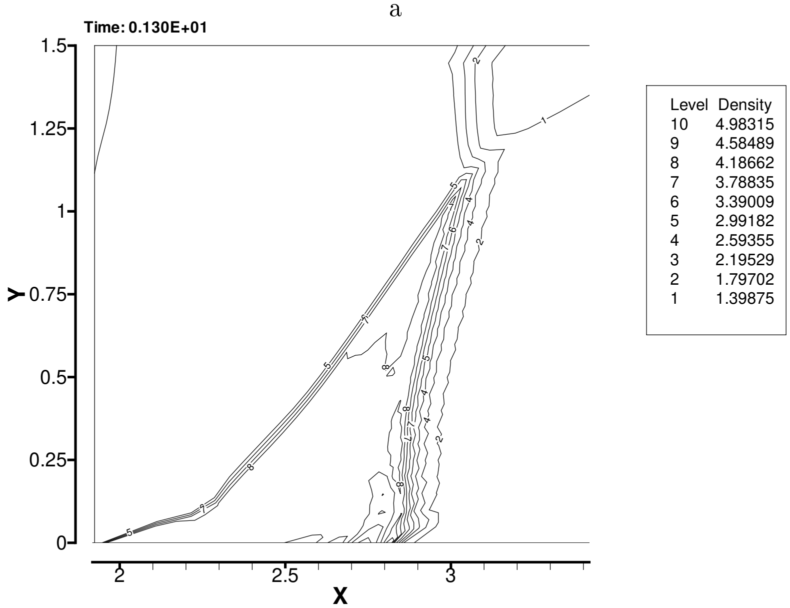

b

Fig. 43: Dukowicz problem results for edge viscosity, merit factor = 0.1. (a) Mesh. (b) Density contour plot.

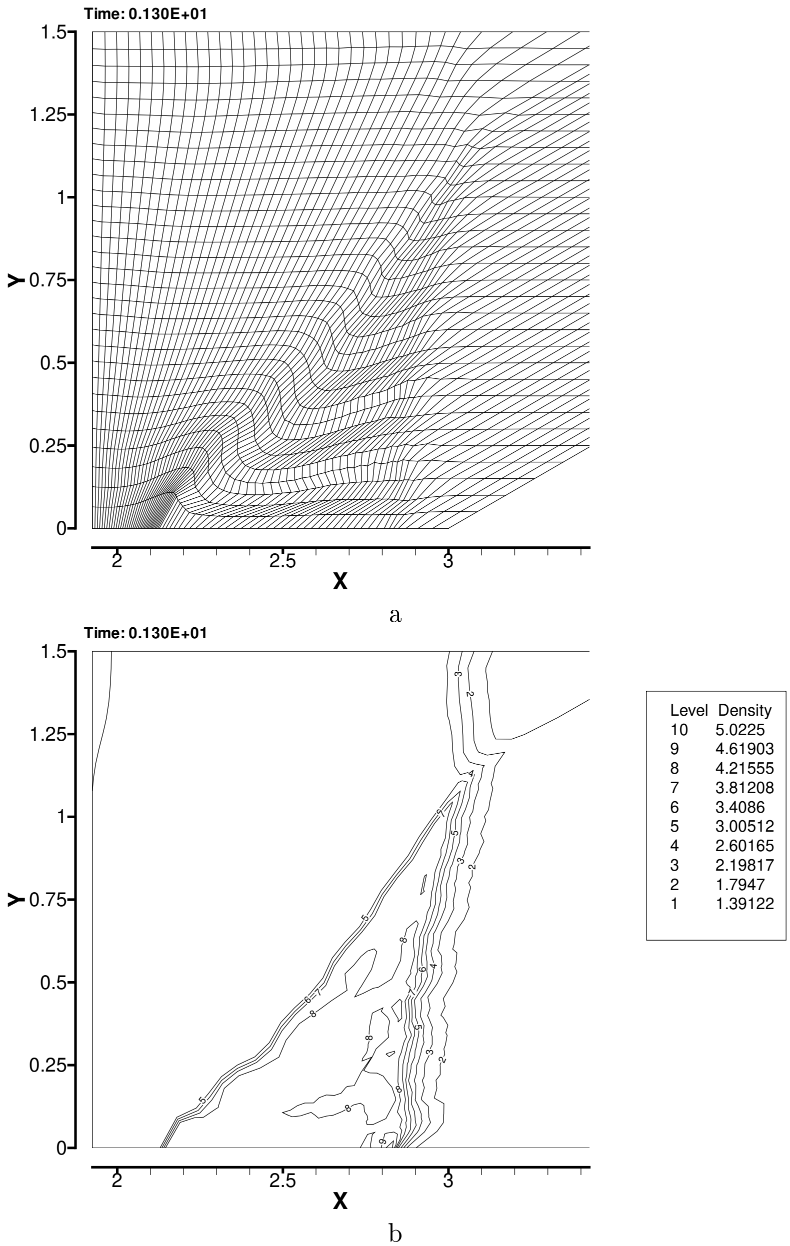

Fig. 44: Dukowicz problem results for symmetric tensor tangential viscosity, merit factor = 0.1. (a) Mesh. (b) Density contour plot.

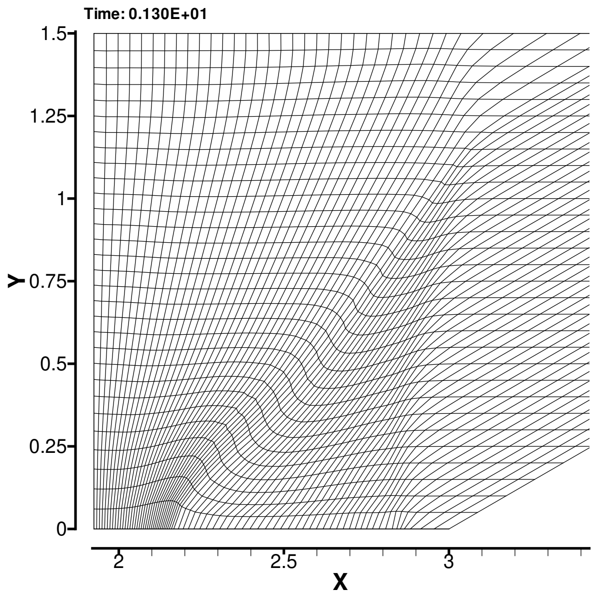

a

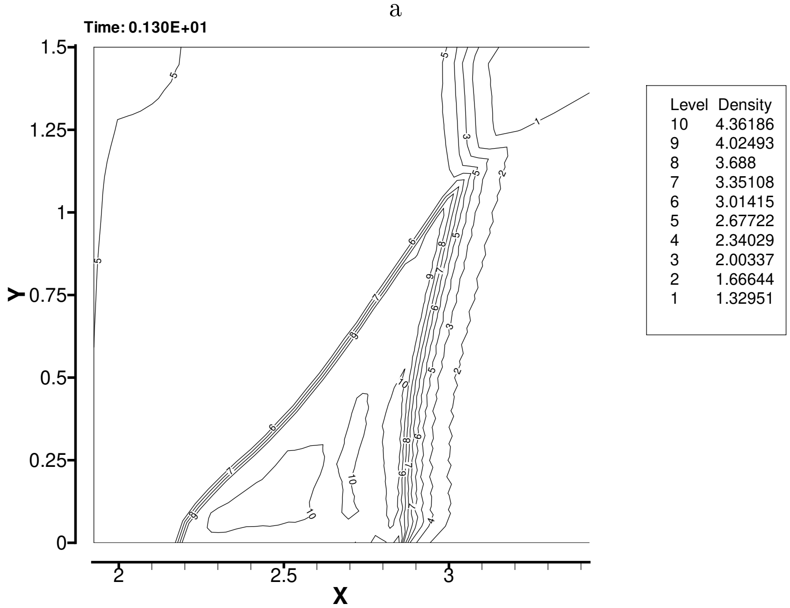

b

Fig. 45: Dukowicz problem results for nonsymmetric tensor tangential viscosity, merit factor = 0.1. (a) Mesh. (b) Density contour plot.

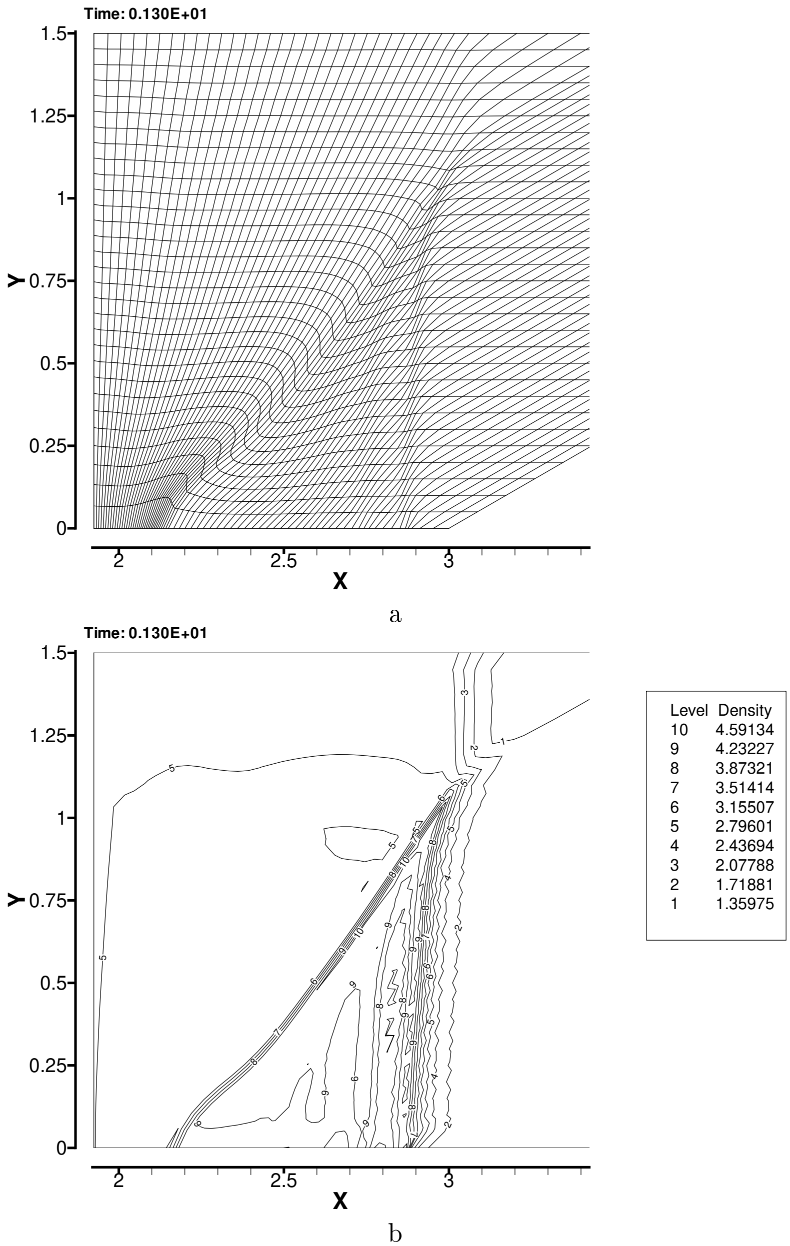

Fig. 46: Dukowicz problem results for tensor normal viscosity, merit factor = 0.1. (a) Mesh. (b) Density contour plot.

The edge viscosity only fails on one of the test problems considered, the Noh problem on a Cartesian mesh. However it does not always produce a smooth mesh, this is seen for the 2:1 Saltzman and Dukowicz problems, though for Dukowicz increasing the subzonal pressures merit factor improves the mesh. The tensor tangential viscosity gives a smooth mesh for all the problems, and gives equal or better agreement to the analytical results then the edge viscosity. The tensor normal viscosity does not fail for any of the problems, but on the Sedov and Dukowicz problems the results are worse than for the edge viscosity.

The disadvantages of the new viscosities are their added complexity and computational cost. The edge viscosity is a simple viscosity that avoids the need for calculating length or velocity change in the shock direction. By choosing to start from the velocity gradient tensor we have had to introduce a critical length into the formulation. For the tensor normal viscosity the length and velocity change for the edge worked well, but for the tensor tangential viscosity it was necessary to use more complex definitions.

8 Conclusion

We have developed an artificial viscosity that satisfies a set of conditions set out by Caramana et al. [6]. The viscosity is based on discrete approximations of the symmetric or nonsymmetric velocity gradient tensor. Due to the tensor nature of the new viscosity, it reduces the dependence of the numerical solution on the grid. This is seen most clearly in results for the Noh problem on an initially square mesh, and the Sedov problem on an initially rectangular mesh.

We have extended the mimetic discretization approach for general grids to tensor operators, deriving expressions for the gradient of a vector and divergence of a tensor. We have then used these discrete operators in an artificial viscosity. These operators can be used for any application where the gradient of a vector and divergence of a tensor is required.

Two artificial viscosities have been developed, both based on the gradient of velocity tensor. The principal difference between the two is in the form of the discrete equations used. Due to the discrete operators used, both viscosities are more complex and computationally expensive than the edge viscosity.

Choosing to start from the gradient of velocity tensor means that the viscous force continuity condition has not been completely satisfied as there is no clear method of doing so.

There are two main areas for future work. The first area is investigating different possibilities for viscosity coefficient and limiter function, as the test showed that these can have a strong effect on the results. This includes investigating forms of the coefficient that do fully satisfy the viscous force continuity condition. The second area is extending the viscosity to work with unstructured meshes.

Acknowledgements
We thank E. Caramana and L. Margolin for their useful comments and suggestions.
This research is supported by the Department of Energy, under contract W-7405-ENG-36.

References

[1] J. Von Neumann and R.D. Richtmyer. A method for the calculation of hydrodynamic shocks. *Journal of Applied Physics*, 21:232–237, 1950.

[2] R. Landshoff. A numerical method for treating fluid flow in the presence of shocks. Technical Report LA-1930, Los Alamos National Laboratory, 1955.

[3] M.L. Wilkins. Use of artificial viscosity in multidimensional fluid dynamic calculations. *Journal of Computational Physics*, 36:281–303, 1980.

[4] V.F. Kurapatenko. *In: Difference methods for solutions of problems of mathematical physics, I (Editor: N.N. Janenko)*, page 116. Amer. Math. Soc., Providence, R.I., 1967.

[5] D.J. Benson. A new two-dimensional flux-limited shock viscosity for impact calculations. *Computer Methods in Applied Mechanics and Engineering*, 93:39–95, 1991.

[6] E.J. Caramana, M.J. Shashkov, and P.P. Whalen. Formulations of artificial viscosity for multi-dimensional shock wave computations. *Journal of Computational Physics*, 144:70–97, 1998.

[7] W.F. Noh. Errors for calculations of strong shocks using an artificial viscosity and an artificial heat flux. Technical Report UCRL-53669, Lawrence Livermore National Laboratory, December 1985.

[8] L.G. Margolin. A centered artificial viscosity for cells with large aspect ratios. Technical Report UCRL-53882, Lawrence Livermore National Laboratory, August 1988.

[9] J.M. Hyman and M. Shashkov. Adjoint operators for the natural discretizations of the divergence, gradient and curl on logically rectangular grids. *Applied Numerical Mathematics*, 25:413–442, 1997.

[10] A.A. Samarskii, V.F. Tishkin, A.P. Favorskii, and M. Yu. Shashkov. Operational finite-difference schemes. *Differential Equations*, 17(7):854–862, 1981.

[11] M. Shashkov and S. Steinberg. Support-operator finite-difference algorithms for general elliptic problems. *Journal of Computational Physics*, 118:131–151, 1995.

[12] M. Shashkov. *Conservative Finite-Difference Methods on General Grids.* CRC Press, Boca Raton, FL, 1996.

[13] M. Shashkov and S. Steinberg. Solving diffusion equations with rough coefficients in rough grids. *Journal of Computational Physics*, 129:383–405, 1996.

[14] J.M. Hyman and M. Shashkov. Natural discretizations for the divergence, gradient and curl on logically rectangular grids. *Computers & Mathematics with Applications*, 33(4):81–104, 1997.

[15] E.J. Caramana, D.E. Burton, M.J. Shashkov, and P.P. Whalen. The construction of compatible hydrodynamics algorithms utilizing conservation of total energy. *Journal of Computational Physics*, 146:227–262, 1998.

[16] E.J. Caramana and M.J. Shashkov. Elimination of artificial grid distortion and hour-glass type motions by means of Lagrangian subzonal masses and pressures. *Journal of Computational Physics*, 142:521–561, 1998.

[17] D.J. Benson and S. Schoenfeld. A total variation diminishing shock viscosity. *Computational Mechanics*, 11:107–121, 1993.

[18] L.I. Sedov. *Similarity and dimensional methods in mechanics.* Academic Press, New York, 1959.

[19] J.K. Dukowicz and B.J.A. Meltz. Vorticity errors in multidimensional Lagrangian codes. *Journal of Computational Physics*, 99:115–134, 1992.